SIGNAL DESIGN AND PROCESSING TECHNIQUES FOR WSR-88D AMBIGUITY RESOLUTION

PART - 3

National Severe Storms Laboratory Report

prepared by: M. Sachidananda,
with contributions by: D.S. Zrnic and R.J. Doviak

July 1999

NOAA, National Severe Storms Laboratory
1313 Halley Circle, Norman, Oklahoma 73069

SIGNAL DESIGN AND PROCESSING TECHNIQUES FOR WSR-88D AMBIGUITY RESOLUTION
Part-3

Contents

SIGNAL DESIGN AND PROCESSING TECHNIQUES FOR WSR-88D AMBIGUITY RESOLUTION

PART - 3

1. Introduction.

The Operational Support Facility (OSF) of the National Weather Service (NWS) has funded the National Severe Storms Laboratory (NSSL), the National Center for Atmospheric Research (NCAR), and the Forecast Systems Laboratory (FSL) to address the mitigation of range and velocity ambiguities in the WSR-88D. This is the third report in the series that deals with velocity and range ambiguity resolution in the WSR-88D. The first two reports mainly dealt with uniform PRT transmission and phase coding techniques to resolve the range ambiguity. Although the phase coding techniques do not directly address the velocity ambiguity problem, its capability of separating overlaid echoes allows the use of shorter PRTs which, in turn, diminishes the occurrence of ambiguous velocities. In this third part, we consider the staggered PRT technique and its variants. Because the pulse repetition time is varied in all these schemes, we classify these methods as time coding methods. A comparison of the SZ phase coding technique and the time coding techniques is also carried out to arrive at a best strategy to be adopted for ambiguity resolution in the WSR-88D.

There are several variants of the time coding schemes reported in the literature. Notable among them are (i) staggered PRT technique (Zrnic and Mahapatra, 1985), (ii) spaced pair with polarization coding (Doviak and Sirmans, 1973), (iii) interlaced sampling (Sirmans et. al. 1976; Doviak and Zrnic, 1993), (iv) multi-PRI scheme suggested by Lincoln Lab, MIT, (Chornoboy and Weber, 1994), (v) alternating codes suggested by Finnish scientists (Pirttila et. al., 1999). A detailed discussion on some of the methods is available in the book by Doviak and Zrnic (1984). Conceptually, some of these methods can provide a large unambiguous

velocity and range. However, their practical utility has been limited by three major problems: (a) the difficulty in filtering the ground clutter, (b) resolving overlaid echoes, and (c) obtaining spectral moment estimates with a reasonably low variance. The clutter filtering introduces unacceptably large bias error in velocity estimates in certain Doppler bands, and the overlaid echoes increase the variance of the spectral estimates.

Most promising among the schemes listed in the previous paragraph are the staggered PRT schemes, and they are possible candidates at least for the higher elevation scans in the WSR-88D. Therefore, in addition to examining all the available schemes, extra effort was put in solving the outstanding problems of the staggered PRT schemes; viz., the clutter filtering and improving the variance of the estimates. We shall focus on the staggered PRT scheme in which 2 PRTs are alternately transmitted.

At least half a dozen different ways of processing the staggered PRT samples were examined using simulation procedures, before a successful solution was arrived at. All these methods are not included in this report, but only the successful method has been given. Here we briefly recount the story of investigations that led to the successful solution to the clutter filtering problem. The decreased variance of the spectral moment estimates was an additional gain that results from the new procedure.

To begin with, we started from an examination of the available results in Zrnic and Mahapatra (1985) and Banjanin and Zrnic (1991). Banjanin and Zrnic (1991) have used a pair of filters on uniform sample sequences derived from the staggered PRT sequence. Torres (1998) has investigated the use of an orthogonal polynomial based regression filter on the non-uniform staggered PRT samples directly. These efforts have indicated that the rejection bands are not easily removed. This is because the problem is in the non-uniform sampling itself and not in the clutter filtering method. The non-uniform sampling produces aliasing of some of the signal power into the clutter spectral regions, and hence, these portions are indistinguishable from the clutter.

The rejection bands in the clutter filter can be traced to the periodicity in the staggered PRT sampling scheme. Therefore, our first approach was to remove the periodicity in the sampling wave form with the hope that this will remove the rejection bands in the clutter filter

or smear the rejection bands over the entire spectrum while greatly reducing the attenuation. There are two ways this could be done: (i) vary the PRTs randomly about some mean value, or (ii) switch between the two PRTs, T_1 and T_2, randomly. In the first case, computation of autocorrelation is complicated; hence, the second method was studied using simulation. It was observed that with randomly switched PRTs, the variance of the velocity estimate is higher ($sd(v)$ was 2 to 3 times larger), and the clutter filter rejection bands do spread out and have a much lower attenuation. The rejection level could be reduced to almost 1dB and spread throughout the spectrum, but at the expense of an increased error in the velocity estimate.

In order to improve the error performance, next we considered spaced pair transmission. The pulse spacing T_1 is made small so that the velocity can be computed from $R(T_1)$ directly rather than using the difference, as in the staggered PRT scheme. Although it is well known that signal overlay cannot be avoided in this case unless polarization switching is used, we encounter other problems such as isolation between the two channels, differential propagation phase shift, etc., which need to be considered in evolving an algorithm for spectral moment estimation. Therefore, the spaced pair scheme was considered without the polarization switching, and with the hope that some kind of phase coding can be worked out to separate the overlaid signals once an effective way of clutter filtering is designed. The advantage seen here is the lower $sd(v)$ available with a spaced pair.

A successful clutter filtering procedure was developed for the spaced pairs scheme, which involved polynomial interpolation to reconstruct an equivalent uniform PRT sequence from the spaced pair sequence of complex samples. Since the clutter signal is of low frequency, the reconstruction is very good; therefore, a spectral domain filter can reduce the bias error in the velocity estimate to a reasonably low value while still maintaining a low $sd(v)$. However, we could not make much headway in separating the overlaid signal with phase coding, without which the spaced pairs scheme is not useful in practice.

The polynomial interpolation was then tried on the staggered PRT sample sequence, but with much less success. The clutter filtering was effective, but the rejection bands in the frequency response of the clutter filter, which produced large bias errors in the velocity estimate, were still present. In all the simulation studies of the clutter filtering, it was observed

that the bias error is systematically negative for positive velocities and positive for negative velocities. It was logical to look for a clutter filtering scheme which produced an exactly opposite bias so that it can be canceled. The result of this search produced the new algorithm.

A major turning point in the search for a clutter filtering method occurred when we started looking at the staggered PRT signal in the spectral domain. This gave us an insight into the spectral properties of the staggered PRT signal which subsequently lead to the development of an effective clutter filtering scheme and also resulted in an improvement in the spectral moment estimates. Thus, two problems were solved at the same time. The new algorithm developed for the staggered PRT scheme overcomes the problem of clutter filtering completely. The algorithm also estimates the spectral moments with much lower variance than that reported earlier. With this new algorithm, it becomes practical to use the staggered PRT scheme to achieve a larger unambiguous velocity and range with acceptable error levels in the Doppler spectral moment estimates.

Although the study was started with an intention of an in depth examination of other available time coding schemes (e.g., the block staggered, spaced pair with polarization switching, etc.) to evaluate their suitability to the WSR-88D ambiguity problem, the discovery of the new clutter filtering and spectral processing method, whose performance surpassed all our expectations, has prompted a change in the emphasis so that a major part of the report is devoted to the delineation of the new algorithm for the staggered PRT scheme and its performance.

2. The staggered PRT technique.

Here, we describe the staggered PRT scheme briefly before we embark on a discussion of the new method of processing. In the staggered PRT technique (Zrnic and Mahapatra, 1985), two different pulse spacings, T_1 and T_2, are used alternately (Fig. 2.1a). Then, alternate pairs of return samples are used to compute autocorrelation estimates, R_1 at lag T_1 and R_2 at lag T_2. The velocity is estimated from the phase difference between the two using the formula,

$$\hat{v} = \lambda \, arg(R_1 R_2^*) \, / \, [4\pi(T_2 - T_1)] \, . \qquad (2.1)$$

Thus, the difference in PRT, (T_2-T_1), determines the unambiguous velocity, v_a, for the staggered PRT technique and is given by

$$v_a = \pm \lambda / [4(T_2-T_1)] \; ; \quad T_1 < T_2 \, . \tag{2.2}$$

Zrnic and Mahapatra (1985) suggest a testing procedure to estimate mean velocity and signal power for echoes received within the time delay (T_1+T_2). In theory, this seems to be possible because the overlaid signals in any two consecutive samples are from two different ranges and, therefore, are uncorrelated. Thus, the expected value of the overlaid signal contribution to the autocorrelation is zero, and the effective unambiguous range becomes

$$r_a = c(T_1+T_2)/2. \tag{2.3}$$

Eq. 2.1 and 2.3 suggest that the staggered PRT is equivalent to a uniform PRT = (T_1+T_2) for the unambiguous range and a uniform PRT = (T_2-T_1) for the unambiguous velocity, and each can be selected independently. However, the practical utility of this scheme is limited due to the quality of estimates. The overlaid signal increases the variance of the estimates because it acts as noise. Thus, the ratio of the overlaid signal powers is the equivalent signal-to-noise ratio (SNR), and for a reasonable accuracy of the estimates, the unwanted signal has to be at least 3 dB below the desired signal power.

Let $r_{a1} = cT_1/2$ and $r_{a2} = cT_2/2$ so that $r_a=r_{a1}+r_{a2}$. If r_{a1} is chosen sufficiently large so that no echoes are received from ranges greater than r_{a1}, then the problem of overlaid echoes could be eliminated. For weather radars, r_{a1} would have to be 460 km (for 0.5 deg. elevation scan), but this would degrade the variance of the estimates considerably. Thus, the practical limit for r_{a1} is smaller than 460 km unless some means of separating the overlaid signals is employed. It may be possible to extend the unambiguous range to r_{a2} with some additional processing to resolve the resulting single signal overlay (i.e., alternate samples only have overlaid echoes) in some of the range gates. This possibility will be explored in the future, but in this report, we consider data which have no overlay.

It is shown by Zrnic and Mahapatra (1985) that the standard error in the velocity estimate increases as the ratio $\kappa = T_1/T_2$ approaches unity, and a good choice is κ =2/3. Thus, the unambiguous range and unambiguous velocity are indirectly tied in practice via the estimate accuracy. However, compared to the uniform PRT, it is possible to achieve a much larger r_a and v_a because the limiting equation is $v_a\, r_{al} = [\kappa/(1-\kappa)]c\lambda/8$ for the staggered PRT scheme.

A major problem with staggered PRT scheme has been the ground clutter filtering. The non-uniform sampling aliases power from certain Doppler frequencies into the clutter frequency band around zero Doppler. Then, filtering the clutter also removes the aliased signal power from a band of spectral coefficients and introduces phase perturbations at these bands which bias the velocity estimate. The widths of these bands depend on the spectrum width of the signal as well as the clutter filter width. Banjanin and Zrnic (1991) have investigated several methods of ground clutter filtering to mitigate the phase perturbations. A scheme they proposed uses two filters sequentially such that the overall filter coefficients are time varying. In the Doppler bands where the filter phase response is not linear, special decision logic corrects velocity estimates. To overcome these obstacles, Chornoboy (1993) proposed a processing technique applied to a block staggered sampling and a least squares design of a filter matrix to achieve a desired frequency response. The added complexity of the pulse pattern enables an improved balance between the magnitude and the phase response so that Chornoboy(1993) achieved satisfactory results.

In the following sections, we present a different and novel approach to the clutter filtering and spectral moment estimation for the staggered PRT sequence.

3. A new approach to processing the staggered PRT samples:

In the proposed new approach, we seek to reconstruct the spectrum of the weather signal from the staggered time series samples, i.e., reconstruct the spectrum of the time series with a uniform sampling period of T_u, starting from the staggered PRT samples sequence, and then estimate the spectral moments from this reconstructed spectrum. This procedure allows estimation of the spectral moments with a much lower variance than the earlier methods. Further, a novel method of clutter filtering in the spectral domain has been proposed which can

achieve a clutter suppression in excess of 40 dB and near complete elimination of all the spurious rejection bands in the $\pm v_a$ interval encountered by other methods of clutter filtering. This is the most important feature of the clutter suppression scheme which makes it practical to use the staggered PRT scheme in weather radars. The processing procedure has two major parts, 1) the reconstruction of an equivalent uniform PRT sequence for spectral moment estimation, and 2) the clutter filtering and residual bias removal. These two are interleaved because the clutter has to be filtered before the spectral moments are estimated. We will explain the reconstruction of the equivalent uniform PRT sequence first however, and then proceed to explain the clutter filtering procedure. These two procedures are incorporated in the algorithm presented later in this report.

3.1. Reconstruction of the signal spectrum.

Our technique requires a small restriction on the selection of the two PRTs used in the staggered PRT transmission. If T_1 and T_2 are the PRTs, we select them such that they are integer multiples of some basic PRT T_u, so that $T_1=n_1T_u$, and $T_2=n_2T_u$, where n_1 and n_2 are integers. Although n_1 and n_2 can be any integers in general, a good choice is $n_2=n_1+1$ from the point of the performance of the staggered PRT scheme. Thus, $(T_2-T_1)=(n_2-n_1)T_u$ determines the unambiguous velocity, v_a, and the unambiguous range, $r_{a1}=cT_1/2$. This, of course, assumes that T_1 is chosen sufficiently large so that no second trip overlay occurs.

Let g_i, i=1,2,3,...M, (M even) be the samples of the weather signal sampled at time intervals T_1 and T_2, alternately. We introduce zeros in g_i to form a sample sequence v_i of length $N=(n_1+n_2)M/2$ with a uniform sampling period of T_u, in which the missing samples are represented by zeros (see Fig. 2.1b). We call this the derived time series. Let c_i be a code sequence of length N obtained by replacing all the g_i samples in v_i by unity. For example, c_i =[1010010100... etc.] for $\kappa = T_1/T_2 = n_1/n_2 = 2/3$. We can write the sample sequence v_i as a product of the sequence c_i and e_i, where e_i is the signal time series sampled at T_u intervals.

$$v_i = c_i\, e_i \;; \qquad i=1,2,3,\ldots N. \tag{3.1}$$

Having converted the staggered PRT sequence into a uniformly sampled sequence (with missing samples represented by zeros), we can examine the spectrum of the uniform sequence, e_i. Thus, the spectrum of v_i can be represented as a convolution of the spectrum of the code c_i and the spectrum of the complete but unknown signal e_i.

$$\text{DFT}(\, v_i \,) = \{\, \text{DFT}(\, c_i \,) \star \text{DFT}(\, e_i \,) \,\} \tag{3.2}$$

where $\star$ represents circular convolution, and DFT( ) represents the discrete Fourier transform of the sequence in brackets. We use the capital letters to denote the spectral coefficients of the corresponding time domain quantities denoted by lowercase letters and capital bold face letters to denote matrices. Subscript index '*i*' is used for the time domain quantities, and subscript index '*k*' is used for the spectral coefficients. For example, E_k = DFT(e_i), are the spectral coefficients, and **E** is the column matrix of coefficients E_k . Eq. (3.2) can be written in matrix form as

$$\mathbf{V} = \mathbf{C}\,\mathbf{E}. \tag{3.3}$$

V and **E** are (Nx1) column matrices containing the spectral coefficients, V_k and E_k, of the corresponding time sequences, v_i and e_i, and **C** is the convolution matrix (size: NxN) whose column vectors are cyclically shifted versions of C_k . To preserve the power in the spectrum, the convolution matrix, **C**, is normalized such that each column vector is a unit vector (i.e., the norm of each column vector is unity). Note that by normalizing the column vectors, the row vectors are also normalized automatically. Our objective here is to reconstruct the spectrum E_k from the samples g_i. It is observed that the convolution matrix is singular (rank of **C** equals the number of staggered PRT samples, M), and hence, it cannot be inverted to get E_k. If we discard the phases of the convolution matrix elements, the matrix becomes non-singular. It may be noted that the magnitude of the spectral coefficients $abs\{E_k\}$ is sufficient to compute the autocorrelation $R(T_u)$, and hence, the velocity and spectrum width. Therefore, we attempt to retrieve abs(**E**) using abs(**C**), which can be inverted.

In general, $abs\{\mathbf{CE}\} \neq abs\{\mathbf{C}\}abs\{\mathbf{E}\}$ because of the complex addition of the coefficients in the process of matrix multiplication. However, because the convolution matrix, **C**, has only (n_1+n_2) non-zero coefficients separated by $N/(n_1+n_2)$ coefficients for $\kappa = n_1/n_2$ in each row (or column), we can show that the complex addition does not take place in the process of convolution if the signal spectrum is narrow so that its spread is less than $N/(n_1+n_2)$ coefficients, and hence, the equality is valid. Then, the convolved matrix **V** has (n_1+n_2) spectral replicas of the original spectrum, **E** (in the complex domain, each replica has a specific complex multiplier), and these replicas do not overlap. Thus, we define a "magnitude deconvolution" as

$$abs\{\mathbf{E}\} = [\ abs\{\mathbf{C}\}]^{-1}\ abs\{\mathbf{V}\}, \tag{3.4}$$

where $[\ abs\{\mathbf{C}\}]^{-1}$ is the magnitude deconvolution matrix. It is important to note that this equation provides the exact magnitude spectrum only under the condition that the non-zero spectral coefficients of the signal e_i spread at most $N/(n_1+n_2)$ coefficients or that the total spread must be less than

$$2v_a/(n_1+n_2) \tag{3.5}$$

in the velocity domain. This condition means the spectrum cannot alias on itself and is obtained from the average sampling rate $2/(T_1+T_2)$ for the staggered sequence. Although wider spectra are not reproduced with high fidelity using this procedure (because of the overlap of spectral coefficients in the spectrum V_k), the non-ideal reconstruction of wider spectra does not generally bias the velocity estimate but affects its variance. If T_1 and T_2 are judiciously chosen, the criterion (Eq. 3.5) can be nearly satisfied for most weather signals. For example, at a 10 cm wavelength and $v_a = \pm 50$ m s^{-1}, Eq. 3.5 can be nearly satisfied for width, $w<6$ m s^{-1}. Nonetheless, it is important to note that the criteria is not satisfied exactly even for $w=4$ m s^{-1}.

Most of the results presented in this report are based on simulation studies. All the computations were carried out using simulated staggered PRT time series. The staggered PRT

sequence is generated from a simulated uniform sample sequence by dropping the missing samples. The time series simulation procedure is explained in Part-1 of this report. There is an inherent rectangular window associated with a finite sample sequence in practice. This effect is simulated by generating a long time series and then truncating it. The effect of the rectangular window is to spread the power in the spectral domain, resulting in overestimation of the spectrum width. To obtain the true spectrum width, it is necessary to multiply the time sequence by a suitable tapered window function before processing. For Gaussian spectra the von Hann window function works very well.

Fig. 3.1 illustrates the spectrum reconstruction using a simulated weather signal time series. A 10 cm wavelength is assumed, and the magnitude spectrum of the signal time series (signal sampled at a uniform sampling period of T_u=0.5 ms) is shown in Fig. 3.1a. The normalized magnitude spectrum of the code for staggered PRT sampling with κ =2/3 (code is 1010010100...etc.) is shown in Fig. 3.1b. If the staggered PRT sampling were used (T_1=1 ms, T_2=1.5 ms), the spectrum of the derived uniform time series would be as given in Fig. 3.1c, which is the convolution of the first two spectra. The last spectrum (Fig. 3.1d) is the reconstructed spectrum from the staggered PRT samples using the magnitude domain deconvolution procedure. Note that for w=4 m s^{-1}, the spectrum does not exactly satisfy the criteria (3.5); hence, a few residual spectral coefficients remain throughout the spectrum. For larger width signals, the residuals can be significant because of the spectrum overlap, but this is not a cause for concern because the residuals maintain a symmetry about the mean Doppler, and hence, do not bias the mean velocity estimates. The residuals do bias the width estimates, and the spectrum needs to be modified a little by dropping some of the coefficients before the width is estimated. Specifically, for κ=2/3, dropping all the spectral coefficients outside a 2/5th of the spectral coefficients centered on the mean Doppler produces the best width estimates; a small bias remains at widths larger than 6 m s^{-1}. The spectrum width is computed using Eq. 6.37 of Doviak and Zrnic (1993). It is important to note that the velocity is estimated with all the coefficients before truncating the spectrum, and this estimated velocity is used for determining the extent of spectrum to be retained for width computation. The velocity computed from the truncated spectrum will have larger errors (variance as well as bias), and hence, only

the width is computed after truncating the spectrum.

Once the magnitude spectrum is obtained, the spectral domain equivalent of the pulse pair algorithm can be used to estimate the mean power, p, mean velocity, v, and spectrum width, w. The autocorrelation, $R(T_u)$, can be expressed as

$$R(T_u) = 1/N \sum_{k=1}^{N} |E_k|^2 \, e^{j2\pi(k-1)/N}, \qquad (3.6)$$

and the velocity is obtained from the phase of $R(T_u)$. The conventional pulse pair algorithm can be used for mean power and width estimation. Since the time series is obtained by inserting zeros in place of missing samples, a correction factor of $(n_1+n_2)/2$ has to be applied to get the correct mean power estimate. But it is best to obtain signal power from the original staggered PRT samples directly if the clutter filtering procedure (explained later in this report) is not applied. If the ground clutter is present in the time series, the signal power estimation must be done after the clutter filtering and bias removal procedures.

An important advantage of this procedure is that the estimate variances are much lower compared to the method using $R(T_1)$ and $R(T_2)$. Because the procedure is non-linear, it was deemed that the derivations of the theoretical expressions for the variance of the estimates would be too laborious, and the results would be only approximately valid. Therefore, we chose simulations to obtain the standard errors of the velocity estimate, $sd(v)$, and other statistical parameters. Results from one typical simulation run is presented in Fig. 3.2, which shows estimated velocity versus the input velocity. Each point on the figure represents one realization, and the continuous curve is the mean value. Figs. 3.3 and 3.4 show the bias in the estimated width using the simulation procedure without and with the von Hann window. The figures also show that the standard error in the width estimates is small. Each point is one realization, and the continuous curve shows the bias in the width. There is an overestimation of the width for narrower signals without the von Hann window. With the von Hann window weights applied, this bias is removed, and the estimates are better. However, for velocity estimation, it is not necessary to apply the window; in fact, the velocity estimates have lower variance without the window than with the window applied because some information is lost. If one estimated the

spectrum width without using the von Hann window, but accounted for the bias by some other means, the variance of the width estimate also would be lower. If clutter is present and is to be filtered, then application of the von Hann window weights becomes necessary.

The standard errors of the spectral moments obtained from the conventional method and the present method (using the magnitude deconvolution) are compared in the next two figures. In Fig. 3.5, the variation of *sd(v)* as a function of the spectrum width is plotted for (a) the pulse pair velocity estimator that uses the complete time series with a sampling period T_u and length N, (b) the proposed method using the reconstructed spectrum from staggered PRT samples, and (c) the pulse pair velocity estimator that uses the phase of $[R(T_1)/R(T_2)]$. For each spectrum width, a large number of simulations were carried out to obtain the value of the *sd(v)*. There is a significant improvement in the *sd(v)* using the present method, and it compares very well with that of the pulse pair estimator on a complete time series for widths up to 5 m s^{-1}. The spectrum reconstruction is good for widths up to 6 m s^{-1}.

Because the spectrum is reconstructed, it is possible to devise a width estimator which has smaller standard error than what ensues from $log[|R(T_1)/R(T_2)]$. For example, the estimator based on $log[|R(0)/R(T_u)]$ (Eq. 6.37 in Doviak and Zrnic, 1993) yields at least a three fold decrease in the standard error of the estimate - almost the same as the pulse pair estimator using the complete time series. Since the spectrum is reconstructed, reflectivity and width also have similar standard error behavior with respect to the width of the signal. Fig. 3.6 shows the $sd(w)$ computed from extensive simulations. The standard error in the spectrum width estimate also closely follows that of the equivalent uniform PRT.

3.2. Ground clutter filtering.

The clutter filtering is carried out in the spectral domain before the signal spectrum is reconstructed using the magnitude deconvolution procedure described in Section 3(a). The spectrum of the ground clutter returns is assumed to be of narrow width and centered on the zero Doppler. Because the spectrum of the derived time series, v_i, is the convolution of the code spectrum and the signal spectrum, it will have weighted replicas of the clutter spectrum centered on each of the non-zero spectral lines of the code spectrum. The weights are the spectral

coefficients of the code spectrum. An example of the convolved spectrum is shown in Fig. 3.7c for $\kappa = T_1/T_2 = 2/3$. The method to be described is not confined to κ=2/3, but this example is used only to illustrate the clutter filtering procedure. Because the code spectrum in this case has five non-zero spectral coefficients (see Fig. 3.1b), the power from each of the clutter spectral coefficients is spread over five spectral coefficients separated by $N/5$ coefficients in the convolved spectrum. Specifically, power in the k^{th} spectral coefficient is distributed over spectral coefficients at k, $k+M/2$, $k+M$, $k+3M/2$, and $k+2M$, cyclically (i.e., if any of these indices exceed N, subtract N from the number). This type of modulation also affects the weather signal so that its spectrum, too, would be replicated into five bands. The modulation could cause weather and clutter that did not overlap in the unmodulated spectrum to overlap after modulation. In general, the power in each spectral coefficient is spread into only (n_1+n_2) coefficients separated by $N/(n_1+n_2)$ coefficients. Therefore, we can take (n_1+n_2) coefficients at a time and try to restore the spectrum. This is done by rearranging the matrices as described below.

Consider an example with parameters κ=2/3, M=64 for which N=160. Because the convolution matrix has only five non-zero coefficients in each column (or row), we can recast the matrix Eq. 3.3 in the form

$$\mathbf{V}_r = \mathbf{C}_r \, \mathbf{E}_r, \tag{3.7}$$

where subscript 'r' is used to represent rearranged matrices, which are given by

$$V_r = \begin{bmatrix} V_1 & V_2 & V_3 \cdots V_{32} \\ V_{33} & V_{34} & V_{35} \cdots V_{64} \\ V_{65} & V_{66} & V_{67} \cdots V_{96} \\ V_{97} & V_{98} & V_{99} \cdots V_{128} \\ V_{129} & V_{130} & V_{131} \cdots V_{160} \end{bmatrix}, \tag{3.8}$$

$$C_r = \begin{bmatrix} C_1 & C_{129} & C_{97} & C_{65} & C_{33} \\ C_{33} & C_1 & C_{129} & C_{97} & C_{65} \\ C_{65} & C_{33} & C_1 & C_{129} & C_{97} \\ C_{97} & C_{65} & C_{33} & C_1 & C_{129} \\ C_{129} & C_{97} & C_{65} & C_{33} & C_1 \end{bmatrix}, \tag{3.9}$$

and

$$E_r = \begin{bmatrix} E_1 & E_2 & E_3 \ldots . E_{32} \\ E_{33} & E_{34} & E_{35} \ldots . E_{64} \\ E_{65} & E_{66} & E_{67} \ldots . E_{96} \\ E_{97} & E_{98} & E_{99} \ldots . E_{128} \\ E_{129} & E_{130} & E_{131} \ldots . E_{160} \end{bmatrix}. \tag{3.10}$$

The convolution matrix, **C**, is modified by deleting first all the rows containing zero in the first column and then deleting all columns containing zero in the first row, which reduces it to a 5x5 matrix, $\mathbf{C}_r$, and the other two matrices are rearranged as 5x32 matrices, row wise as in Eq. 3.8 and Eq. 3.10. The Matrix $\mathbf{C}_r$ is singular (its rank is 3), and hence, cannot be inverted; its columns are normalized such that the sum of the magnitudes squared of the elements in each column is unity. (This also normalizes the row vectors.) In the complete time series spectrum, E_k, the clutter is confined to the first and last few coefficients (k=1,2,..q and N-q-2, ... N). But the matrix $\mathbf{V}_r$ would have clutter power spread over the first few and the last few columns.

To filter the clutter from the first few columns of $\mathbf{V}_r$, first estimate the complex amplitude of the clutter vector in the column (which also might contain a signal component). This is accomplished by taking the inner product of the column with the complex conjugate of the first column vector of the matrix $\mathbf{C}_r$. The clutter column vector is constructed by multiplying the first column vector of $\mathbf{C}_r$ by this complex amplitude coefficient, and is then subtracted from the corresponding column vector of matrix $\mathbf{V}_r$. This process is carried out for the first few columns containing clutter. Similarly, the clutter from the last few columns is removed using the last column vector of $\mathbf{C}_r$ in place of the first. This complete operation can be written in matrix notation as

$$\mathbf{V}_f = \mathbf{V}_r - \mathbf{C}_{f1}\, \mathbf{V}_r\, \mathbf{I}_{f1} \quad - \mathbf{C}_{f2}\, \mathbf{V}_r\, \mathbf{I}_{f2}, \qquad (3.11)$$

where $\mathbf{C}_{f1}$ and $\mathbf{C}_{f2}$ are the clutter filter matrices, and $\mathbf{I}_{f1}$ and $\mathbf{I}_{f2}$ are matrices which select the columns to be filtered. These are given by

$$\mathbf{C}_{f1} = \mathbf{C}_1\, \mathbf{C}_1^{t*}, \qquad (3.12a)$$

and

$$\mathbf{C}_{f2} = \mathbf{C}_5\, \mathbf{C}_5^{t*}, \qquad (3.12b)$$

where $\mathbf{C}_1$ is the first column vector of $\mathbf{C}_r$, $\mathbf{C}_5$ is the last column vector (5^{th} column for κ=2/3) of $\mathbf{C}_r$, the symbol * indicates complex conjugate, and the superscript "t" stands for transpose. The matrix $\mathbf{I}_{f1}$ is a $M/2$x$M/2$ diagonal matrix with diagonal elements unity for the first q elements and the rest zeros. Similarly, the matrix $\mathbf{I}_{f2}$ is a $M/2$x$M/2$ diagonal matrix with last (q-1) elements unity and the rest zeros. For example, the diagonals of the matrices for q=4 are

$$diag\ \{\mathbf{I}_{f1}\} = [11110000\ \ldots\ 000],$$

and

$$diag\ \{\mathbf{I}_{f2}\} = [0000\ \ldots\ 000111]. \qquad (3.13)$$

These matrices determine the clutter filter width. Note that $(2q\text{-}1) = n_c$ is the number of

columns containing the clutter we wish to filter, or it is the clutter filter width in terms of the number of spectral coefficients. This number should be determined from the expected width of the clutter signal. The matrix operation indicated in Eq. 3.11 produces the filtered signal matrix $\mathbf{V}_f$.

Now, to reconstruct the magnitude spectrum of the weather signal, apply the magnitude deconvolution procedure to $\mathbf{V}_f$, as explained earlier (see Eq. 3.4). This can be done in the rearranged matrix form by inverting Eq. 3.7, and is given by

$$\mathbf{E}_r = [abs\{\mathbf{C}_r\}]^{-1}\ abs\{\mathbf{V}_f\}. \qquad (3.14)$$

This is faster than using Eq. 3.4 because it involves inverting a 5x5 matrix in place of the NxN matrix. The magnitude spectrum $abs\{\mathbf{E}_r\}$ is rearranged in a column matrix $\mathbf{E}_s$. The autocorrelation $R(T_u)$ is calculated from the magnitude coefficients of $\mathbf{E}_s$ using Eq. 3.6, and the velocity estimate from the phase of $R(T_u)$.

In Fig. 3.7 is an illustration of the clutter filtering procedure using a simulated signal and for the clutter-to-signal power ratio of 40dB. The spectrum of the complete signal (Fig. 3.7a) sampled with a period of $(T_2\text{-}T_1)$ is what we want to reconstruct from the staggered PRT samples. The clutter spectrum alone is in Fig. 3.7b. The spectrum of the signal plus clutter computed from the staggered PRT samples (or the derived uniform sequence) is in Fig. 3.7c. Note that the clutter is spread over five bins across the spectrum. The signal is not visible because it is 40 dB below the clutter. The spectrum after the clutter is filtered is given in Fig. 3.7d. The signal spectrum reconstructed by the magnitude deconvolution (Fig. 3.7e) has some residuals at the locations where clutter was present. Note that the residual coefficients at the places where clutter was removed all have the same amplitude; viz., coefficients # 1, 33, 65, 97, and 129 have the same amplitude; coefficients # 2, 34, 66, 98, and 130 have the same amplitude, etc. This fact and its relation to the actual signal amplitude is used later to remove the velocity bias. The spectrum after the residuals are deleted (Fig. 3.7f) is nearly the same as the original spectrum except for a few coefficients at the tail ends, and the coefficients from which clutter is filtered will also have an amplitude error which causes the bias.

Because the columns of $\mathbf{C}_r$ are not orthogonal, clutter filtering also filters some part of the signal power from the corresponding spectral coefficients. The signal component removed is the projection of the signal vector onto the clutter vector, and this results in an alteration of the relative amplitudes of the signal vector elements. Therefore, the vector does not deconvolve back into a single signal coefficient in the magnitude deconvolution process but produces residual spectral coefficients at the locations where clutter was present. However, the amplitudes of these residuals are comparable or less than the signal coefficients. The residuals do produce a small bias in the mean velocity estimate which is not appreciable for small clutter filter widths. The residuals are zero if the signal spectrum and the clutter spectrum do not overlap in the spectrum of staggered PRT sequence; if there is an overlap, the residuals can be significant compared to the signal coefficients but are nearly symmetrically placed about the mean velocity, hence produce a small bias. The maximum bias produced by the small asymmetry is about ±2 m s^{-1} for a clutter filter width of 4.4 m s^{-1}, $\kappa = 2/3$, and $v_a = 50$ m s^{-1}. For larger filter width, the bias increases proportionately, and systematically cycles between positive and negative maximum values as a function of the mean velocity. There are no significant dropouts in the velocity recovery. This very important feature of this clutter filtering procedure implies that the clutter filter response has no spurious rejection bands. The resulting velocity estimates might be good for some applications, but even this small bias can be removed by some additional processing as explained later in this section. The spectrum width estimate is heavily biased because of the residuals. A major part of the spectrum width bias is removed by deleting all the spectral coefficients outside $\{2N/(n_1+n_2)\}$ coefficients centered on the mean velocity, and then computing the spectrum width. It is the part of the bias produced by the residual spectral coefficients due to the spectrum overlap in the staggered PRT signal spectrum, as explained in the previous section (Section 3.a). There is also an additional bias produced because of the clutter filtering. This bias is comparable to that in the velocity and is a function of the mean velocity. This part of the width bias is eliminated in the process of removing the bias error in the velocity. The clutter filtering procedure also produces a bias in the signal power estimate, which is a function of the mean velocity as in the case of spectrum width bias. This bias also is removed in the bias removal procedure. Thus, the bias removal

procedure removes the bias in all three spectral moment estimates.

This method was tested (without the bias correction part) using simulated staggered PRT weather signals with an unambiguous velocity interval of ±50 m s^{-1} and κ=2/3. Fig. 3.8 shows the mean estimated velocity as a function of the input velocity for one specific set of parameters indicated in the figure. All the published methods of clutter filtering produce clutter filter notches at velocities ±20 m s^{-1} and ±40 m s^{-1} (locations corresponding to the first and second alias of the sampling frequency $(T_1+T_2)^{-1}$) in addition to the notch at zero Doppler. Note that the velocity recovery is accurate at these values in the present method. There is a small bias between two of these notch locations because of the residual coefficients at spectral locations from which the clutter was removed, but it is within about ±2 m s^{-1}, and hence, would be acceptable for some applications. The bias error is maximum for mean velocities ±5, ±15, ±25, ±35, and ±45 m s^{-1}, and it is zero for ±10, ±20, ±30, ±40, and ±50 m s^{-1}. In Fig. 3.9, the bias and the standard deviation of the velocity estimate is shown for the same set of parameters in an expanded scale. There is a small increase in the standard error whenever the signal spectrum and the clutter spectrum overlap (i.e., at velocities 0, ±20, and ±40 m s^{-1}). For all these simulations, the clutter filter width used is $2v_a(9/160)$ (i.e., 9 coefficients out of 160 are removed). This is the filter width required to effectively remove clutter for a CSR =30 dB. For larger CSR values, clutter filter width also needs to be increased, and this produces larger bias error in the velocity estimate. Fig. 3.10 shows normalized maximum bias error in the velocity as a function of normalized clutter filter width, $(w_f/2v_a)$, obtained using a large number of simulations. The clutter filter width required for effective removal of the clutter, as judged by the velocity estimate quality, is given in Fig. 3.11. ($\zeta=w_f/w_c$; w_f is the clutter filter width, and w_c is the clutter spectrum width.) From these two figures, it can be inferred that for a clutter spectrum width of 0.35 m s^{-1} if the CSR is less than about 20 dB, the bias error in the velocity is less than ±1.5 m s^{-1} and might be tolerated. For larger CSR, we need to remove the velocity bias. The curve in Fig. 3.11 indicates that there is an upper limit for the signal velocity recovery in the presence of strong clutter. The CSR seems to level off around 50 dB with increasing width of the clutter filter, and about CSR=45 to 50 dB is about the best that can be filtered. At these highest CSR values, the velocity estimate has large standard error, especially

if the signal and clutter overlap. For larger width signals (w >6 m s^{-1}), the reconstructed spectra are not accurate because of the spectrum overlap; hence, there is an increase in the variance of the velocity estimate.

Fig. 3.12 shows the clutter suppression ratio, $\alpha = -10 \log\{P_{res}/P_{tot}\}$, as a function of the normalized clutter filter width, ζ , ($\zeta = w_f / w_c$; w_f is the clutter filter width, and w_c is the clutter spectrum width) from simulation. The continuous curve is the theoretical curve for a Gaussian signal. Assuming that the clutter suppression ratio required is equal to the *CSR* plus the *SNR* (about 20 dB), we would expect velocity recovery for *CSR*=50dB for a clutter filter width, ζ=20 (see Fig. 3.12). But Fig. 3.11 indicates a velocity recovery only up to about *CSR*=40 dB for this clutter filter width. In fact, the velocity recovery is good up to *CSR*=50dB for regions where the clutter and signal do not overlap, but in the regions of overlap, there is an increase in the *sd*(v) which sets an upper limit of *CSR*=40 dB.

The clutter filtering produces a bias in the width estimate as shown in one sample plot in Fig. 3.13 for an input width of 4 m s^{-1}. The points show each realization, and the mean value from several simulations is the continuous curve. It is clearly seen that the bias is a function of the mean velocity. This pattern continues for any input width. The amplitude of the bias in the width estimate is a function of the clutter filter width. This bias also is removed in the process of removing the bias error in the velocity discussed later in this section. The figure also shows the standard error in the width estimate which is less than 1 m s^{-1}.

3.3. Bias removal procedure.

It is mentioned in the previous paragraph that the clutter filtering from a column of the $\mathbf{V}_r$ alters the relative amplitudes of the signal components present in the column, thus preventing it from deconvolving into a single signal component in $\mathbf{V}_f$. A very interesting feature of $\mathbf{V}_f$ is that the amplitude of all the elements of the column vector from which clutter is filtered is modified such that after the magnitude deconvolution, the amplitude of all elements of the column vector is the same. Further, this amplitude bears a fixed amplitude relationship with the actual signal component present in the vector. This amplitude relationship is a function of the correct signal vector. There are 5 signal vectors for κ=2/3 (5 columns of the matrix $\mathbf{C}_r$

). The correct signal vector can be obtained from the estimated mean velocity. The five velocity regions which correspond to the five signal vectors are ($-v_a$ to $-3v_a/5$), ($-3v_a/5$ to $-v_a/5$), ($-v_a/5$ to $v_a/5$), ($v_a/5$ to $3v_a/5$), and ($3v_a/5$ to v_a). If we discard the sign of the spectral components, positive and negative velocities produce the same amplitude relationship. This relationship can be obtained by performing the matrix operations corresponding to the clutter filtering and magnitude deconvolution on each of the unit column vectors, $\mathbf{C}_1$ to $\mathbf{C}_5$, and is given by

$$\xi_k = 1 \,/\, abs\{\ [abs(\mathbf{C}_r)]^{-1}\ [\mathbf{C}_k - (\mathbf{C}_1^{t*}\mathbf{C}_k)\mathbf{C}_1]\}; \quad k=1,2,..(n_1+n_2), \qquad (3.15)$$

where $\mathbf{C}_r$ is the rearranged code matrix defined earlier, $\mathbf{C}_k$ is the k^{th} column vector of $\mathbf{C}_r$, and ξ_k is the ratio of the actual signal amplitude to the amplitude after magnitude deconvolution for the k^{th} velocity region. The ξ_k values are symmetric with respect to the zero velocity; i.e., the positive and negative velocities have the same value (except for the sign which is discarded because we are working in the magnitude domain). Therefore, only the first three values are taken for $\kappa=2/3$. Note that $\xi_1=\infty$, and hence, cannot be used for signal amplitude correction in the region $|v|<v_a/5$.

The ratio of the actual signal amplitude to the residual amplitude, ξ_k, obtained from simulation, is shown in Fig. 3.14 as a function of the input velocity. This is possible because the original signal is known for the simulation. In the staggered PRT processing algorithm, the estimated velocity is used in place of input velocity (Input velocity is available only for simulation!) to select the constant. The two constants for $\kappa=2/3$ are $\xi_2=1.1056$ and $\xi_3=1.789$ for regions $v_a/5<|v|<3v_a/5$ and $|v|>3v_a/5$, respectively. In the region around zero velocity, ($-v_a/5$ to $v_a/5$), the residual component is nearly zero, and hence, the ratio is very large. In and around the transition regions at $|v|= v_a/5$ and $3v_a/5$ (10 and 30 m s^{-1}), there is a rapid change in the constants, but this is of no concern because at these locations, the bias is already zero. (The residual spectral coefficients are symmetrically placed with respect to the mean velocity.) These fuzzy regions widen with increased spectrum width. These ξ values are independent of the number of samples, M, and also the selection of unambiguous velocity, v_a, for a given κ. The three regions of $\pm v_a$ are indicated in Fig. 3.14. For a different κ value, the number of regions

as well as the ξ values for each region are different. (ξ values are given later in the report for other κ.)

The bias removal procedure is to reconstruct the original signal column vector whenever clutter is removed from a column vector of $\mathbf{V}_r$. To do this, first we calculate the mean velocity estimate from the spectrum $\mathbf{E}_s$ and determine the velocity region, (1), (2), or (3), to choose the multiplication coefficient, ξ. To explain the bias removal procedure, let us rearrange $\mathbf{E}_s$ into a (n_1+n_2)x$M/2$ matrix (5x32 for the present example), $\mathbf{E}_{sr}$, in which the first q and the last q-1 columns vectors, from which the clutter is filtered, will have same element values (different values for each column). Set all the elements of these columns to zero except one row. This row is determined by selecting elements in the $N/(n_1+n_2)$ spectral coefficients centered on the mean velocity estimate. Whichever row falls within this interval, the elements of that row of columns 1 to q are **not** set to zero but are multiplied by the constant ξ. Similarly, whichever row falls within this interval for the last (q-1) columns, the elements of that row of the last (q-1) columns are **not** set to zero but are multiplied by the constant ξ. This procedure is applied only if the estimated velocity is in regions (2) and (3), with multiplier ξ_k selected appropriately for the region (see Fig. 3.14 for regions). For region (1), the elements of this particular row, selected as in the previous case, are replaced by the $(q+1)^{th}$ element value for columns 1 to q, and the $(M/2-q+1)^{th}$ value for columns ($M/2-q+2$) to $M/2$. This, of course, is an approximation for want of an accurate ξ value. For this region, the clutter and signal vectors are the same, and hence, the signal is completely removed while removing the clutter. Therefore, we take the signal amplitude from the adjacent coefficient from which clutter is not filtered (e.g., $(q+1)^{th}$ column) and insert this value as an approximate signal amplitude. This, of course, is not the best choice but is taken as the simplest option. The bias removal is not exact for region (1) but is reasonably good for most applications. This corrected $\mathbf{E}_{sr}$ is again rearranged into a single column vector, and $R(T_u)$ and velocity are re-estimated from this column vector. This velocity is without any bias in the $\pm v_a$ interval. Thus, the additional computation to remove the bias error involves some matrix element manipulation and computation of autocorrelation and velocity a second time. The procedure is also applicable to other stagger ratios, κ.

This whole process of bias correction can be put in mathematical form using matrix

operations. We need to program two different procedures, one for the region (1), and the other for the regions (2) and (3). These two procedures are combined into a single matrix equation. The following paragraph explains the different matrices used in the equation.

Let $\mathbf{E}_a$ be a (NxN) diagonal matrix whose diagonal is given by $diag\{\mathbf{E}_a\}= \mathbf{E}_s$, the elements of the column matrix obtained from Eq. 3.14 after magnitude deconvolution. When a matrix is called a diagonal matrix, it is understood that the off diagonal elements of the matrix are all zeros. We modify $\mathbf{E}_a$ into another diagonal matrix $\mathbf{E}_a^m$ (the superscript 'm' stands for modified) in which first q diagonal elements are replaced by $(q+1)^{th}$ diagonal element, and the last $(q-1)$ diagonal elements are replaced by the $(N-q+1)^{th}$ diagonal element. This modification is made for taking care of the region (1) correction. The corrected spectrum is extracted from the diagonal of the corrected matrix $\mathbf{E}_a^c$ which is given by the equation,

$$\mathbf{E}_a^c = \mathbf{E}_a \mathbf{I}_1 + \mathbf{E}_a^m \mathbf{I}_2 \mathbf{I}_v \mathbf{Z} , \qquad (3.16)$$

where the matrices $\mathbf{I}_1$, $\mathbf{I}_2$, $\mathbf{I}_v$, and $\mathbf{Z}$ are all (NxN) diagonal matrices defined by

$$diag\{\mathbf{I}_2\} = [(diag\{\mathbf{I}_{f1}\} + diag\{\mathbf{I}_{f2}\}),\ldots \text{ repeat } (n_1+n_2) \text{ times}], \qquad (3.17)$$

$$diag\{\mathbf{I}_1\} = \text{complement of } diag\{\mathbf{I}_2\}, \text{ (interchange 0s and 1s)}, \qquad (3.18)$$

$$diag\{\mathbf{I}_v\} = [000\ldots\ 001111\ldots1110000\ldots], \qquad (3.19)$$

(N elements with $2N/(n_1+n_2)$ 1s placed such that the 1s are centered on the mean velocity coefficient, the rest are all zeros), and

$$diag\{\mathbf{Z}\} = [1111\ldots,\xi_2,\xi_2,\xi_2\ldots,\xi_3,\xi_3,\xi_3,\ldots\ \ ,\xi_2,\xi_2,\xi_2\ldots,111\ldots] . \qquad (3.20)$$

The construction of $diag\{\mathbf{Z}\}$ needs some explanation. The parameters, ξ_2,ξ_3, etc. are the correction coefficients for the velocity regions (2), (3), etc. The region (1) correction coefficient is set to unity (actually $\xi_1 \to \infty$) because it is not used in the correction scheme. The velocity scale corresponding to the spectral coefficients 1 to N is from 0 to $-v_a$ and $+v_a$ to 0; therefore, the first $N/2(n_1+n_2)$ and the last $N/2(n_1+n_2)$ coefficients are 1s representing the region (1). The next $N/(n_1+n_2)$ coefficients correspond to region (2) and so on up to the center, and then, the same coefficients repeat in the reverse order up to the end. The diagonal is symmetric about the center.

It may be noted that all the matrices used in Eq. 3.16 are diagonal matrices. The matrices were defined that way so that the entire operation can be put in the conventional

matrix operations but it is not necessary to form these (NxN) matrices while programming because it is actually element by element multiplication, the off diagonal elements being zero for all the matrices. Thus, we can define an element by element product of two column matrices as a dot product (like the MATLAB ·* operator), and use diagonals as column vectors in Eq. 3.16, and multiplication replaced by dot operator.

With the bias correction scheme implemented, Figs. 3.8 and 3.9 are regenerated to show the performance of the bias correction scheme. Fig. 3.15 shows the velocity recovery for κ=2/3 and $v_a = \pm 50$ m s^{-1}, and Fig. 3.16 is the plot of bias error and standard deviation of the velocity estimate. It can be observed that while the standard error has not changed, the bias error is nearly zero for the entire $\pm v_a$ interval (compare these figures with Figs. 3.8 and 3.9). The large error at the extremities is because of the velocity aliasing. The procedure also removes the bias error in the width estimate as shown in Fig. 3.17 (compare this with Fig. 3.13 for the same parameters without the bias correction applied).

It was mentioned earlier that the clutter filtering procedure can suppress clutter better than 40 dB, but to obtain this performance, we need to select the clutter filter width judiciously. Larger than required filter width introduces perturbations in the signal spectrum which produces residual bias in velocity estimate. To remove this residual bias, the bias removal part has to be implemented in the algorithm at the cost of some additional computations. If the clutter filter width is made just sufficient to obtain the desired clutter rejection, we get the best performance. If the clutter filter width is further reduced, the clutter suppression may be inadequate, and the residual clutter in the unfiltered columns of $\mathbf{V}_r$ causes a bias error that cannot be removed by the bias removal scheme. Fig. 3.11 shows the clutter suppression ratio, α, as a function of normalized clutter filter width, $\zeta = w_f / w_c$, (normalized with respect to the clutter spectrum width, w_f is the clutter filter width, and w_c is the clutter spectrum width, both in m s^{-1}) for a Gaussian shaped spectrum. This figure can be used as an approximate guide for selecting the optimum clutter filter width, approximate because the actual weather signal is not exactly Gaussian. For the spectral domain clutter filtering algorithm, we need to determine the number of coefficients to be filtered, which is obtained from the formula,

$$n_c = (N\zeta/2v_a)w_c. \qquad (3.21)$$

Since n_c has to be an odd integer for symmetrical positioning of the clutter filter with respect to the zero Doppler, we truncate n_c to the nearest higher odd integer. A ζ value of about 20 to 25 is a good choice for most cases with large clutter signal, although lower values can be used in practice with reasonable suppression. The choice actually should depend on the clutter-to-signal ratio CSR (see Fig. 3.11 for optimum value). Simulation results show that for CSR >40dB, which requires wide clutter filter, the bias error is too large to be completely removed over the entire velocity interval. There are more outliers generated in some regions, especially the regions where the clutter and signal overlap. In these regions, the bias correction also fails because the algorithm uses the estimated velocity (with the bias) to determine the matrix $\mathbf{I}_v$ (in Eq. 3.16).

3.4. Generalization to other κ and v_a values

The method of clutter filtering and bias removal is general and can be adopted to any value of κ and v_a, but the velocity recovery and the clutter filtering performance depend on several factors, such as the number of zeros required to be inserted to derive a uniform PRT sequence, in relation to the available staggered PRT samples, and the selection of T_1 (or r_{a1} or v_a). The smaller the M/N ratio, the lesser will be the information available to reconstruct the spectrum; hence, we can expect the estimate variance to increase for a given v_a. The largest ratio M/N=2/5 is obtained for κ=2/3, and it is the same value as indicated by Zrnic and Mahapatra (1985) for the staggered PRT scheme from the point of variance of the velocity estimate. The next largest M/N=2/7 is obtained for κ=3/4, and the algorithm performs reasonably well but is not as good; it has an advantage of larger r_{a1} for a given v_a. The unambiguous range is tripled at the expense of a poorer performance with respect to the variance of the spectral moment estimates. For comparison, performance of the algorithm for κ=3/4 is given in Figs. 3.18 to 3.21, all for the same v_a=50 m s^{-1} and M=64. Fig. 3.18 shows the velocity recovery for the parameters listed in the figure. The large error at extreme ends is due to the aliasing of the velocity. Compare this figure with Fig. 3.8 for κ=2/3. The $sd(v)$ and bias error in the

velocity estimate are larger compared to that for κ=2/3 (Fig. 3.19). Figs. 3.20 and 3.21 are similar to Figs. 3.5 and 3.6 but are for κ=3/4. These figures give us a general idea of the errors that can be expected for κ=3/4. Note a significant increase in the $sd(v)$ as a function of the width of the signal in Fig. 3.20 (compare with Fig. 3.5), and the spectrum reconstruction provides only a small improvement over the earlier method of velocity computation. The velocity is not usable in practice for widths greater than about 4 m s^{-1}. This is a handicap for κ=3/4 because weather signals in severe storms have a median width of 4 m s^{-1} (Doviak and Zrnic, 1993). Fig. 3.21 shows the error performance of the algorithm with respect to the spectrum width estimation for κ=3/4.

As mentioned earlier, the bias correction scheme can be applied by redefining regions and multiplication factors for each region. Because the code sequence corresponding to κ=3/4 has a periodicity of 7, the velocity interval $\pm v_a$ is divided into four regions, each of which has a corresponding ξ value. The four regions are $|v|<v_a/7$, $v_a/7<|v|<3v_a/7$, $3v_a/7<|v|<5v_a/7$, and $5v_a/5<|v|<v_a$, and the corresponding ξ_k values are ∞, 1.052, 2.364, and 1.312 for k=1, 2, 3, and 4, respectively (calculated from Eq.3.15). Similarly, for κ=4/5, there are five regions and five different values for ξ. The calculated values are $\xi_1=\infty$ for region $|v|<v_a/9$, ξ_2=1.031 for region $v_a/9<|v|<3v_a/9$, ξ_3=2.97 for region $3v_a/9<|v|<5v_a/9$, ξ_4=1.173 for region $5v_a/9<|v|<7v_a/9$, and ξ_5=1.58 for region $7v_a/9<|v|<v_a$. In the first region where $\xi=\infty$, the bias correction procedure does not use the ξ value as explained earlier, and hence, is set to unity in all cases.

The results presented so far indicate that the algorithm can effectively estimate the spectral moments in the presence of the ground clutter for a particular selection of parameters (κ=2/3 and 3/4; T_u=0.5ms; λ=10cm; etc.). Nonetheless, while applying this method to other situations, one has to bear in mind that there are restrictions in the selection of these parameters. One important criteria that determines the usefulness of a procedure is the standard error in the velocity estimate, $sd(v)$, and the bias error, which has to be within a specified tolerance. The restrictions on the selection of parameters are arrived at based on this usefulness criteria. From an examination of Fig. 3.5, it is observed that the $sd(v)$ starts increasing at about w=6 m s^{-1}. For any other selection of T_u (hence v_a), the $sd(v)$ starts increasing at about the same normalized value, $w/2v_a$ (i.e., about 6 percent of $2v_a$). The $sd(v)$ also increases with larger values of κ, as

shown in Fig. 3.20 where the cutoff point for κ=3/4 is at $w/2v_a$ = 0.04 (or 4 percent). If the spectral moments of weather signals of widths up to at least 6 m s^{-1} are to be accurately estimated, we need to restrict the parameters, κ and T_u, to 2/3 and 0.5 ms, respectively. Another criteria in selecting the parameters is the second trip overlay. If overlay is to be avoided and also meet the $sd(v)$ criteria, then the utility of the algorithm is limited to higher elevation scans where these criteria can be met.

3.5. The algorithm

This section describes the spectral parameter estimation algorithm for the Doppler weather radar with staggered PRT transmission scheme step by step. The algorithm is written for any selectable stagger ratio, κ, unambiguous velocity, v_a, and number of samples, M (must be even).

========== begin ==========

1. The transmission of the pulses is at PRTs T_1 and T_2, alternately. The number of samples collected using the staggered PRT scheme is M for each range gate. The PRTs are selected such that $T_1=n_1T_u$, and $T_2=n_2T_u$. Let g_i ; i = 1,2,..., M, be the time series samples.

2. Compute the signal power (and reflectivity) from the original time series g_i, if clutter is not present (omit steps 7 through 10 to remove clutter filter). If clutter is present and is to be filtered, the signal power is computed in step 17.

3. Insert zeros in the time series to derive a uniformly sampled sequence v_i of length $N=(n_1+n_2)M/2$. Zeros are inserted in places of missing samples.

4. Compute the DFT of the derived time series v_i, and rearrange the spectral coefficients into a $((n_1+n_2)$ x $M/2)$ size matrix $\mathbf{V}_r$. The spectral coefficients are arranged row-wise to form the matrix.

5. Compute the DFT of the code, c_i, corresponding to the κ, and form the convolution matrix **C** using the coefficients C_i (see Eq. 3.3).

6. Delete all the rows and columns of **C** containing zero in the first column and row, to get the (n_1+n_2)x(n_1+n_2) rearranged matrix $\mathbf{C}_r$ (see Eq. 3.9).

7. Extract first column $\mathbf{C}_1$ and last column $\mathbf{C}_5$ of $\mathbf{C}_r$.

8. Compute the clutter filter matrices $\mathbf{C}_{f1}$ and $\mathbf{C}_{f2}$ using (Eq. 3.12a and Eq. 3.12b).

$$\mathbf{C}_{f1} = \mathbf{C}_1 \mathbf{C}_1^{t*}$$
$$\mathbf{C}_{f2} = \mathbf{C}_5 \mathbf{C}_5^{t*}$$

9. Determine the clutter filter width, $(2q\text{-}1)$, in terms of the number of spectral coefficients and form the $(M/2$x$M/2)$ diagonal matrices $\mathbf{I}_{f1}$ and $\mathbf{I}_{f2}$, which select the columns that contain clutter signal. (A clutter map can be used for determining the clutter filter width.)

10. Filter the clutter by performing the matrix multiplication and subtraction indicated in (Eq. 3.11).

$$\mathbf{V}_f = \mathbf{V}_r - \mathbf{C}_{f1} \mathbf{V}_r \mathbf{I}_{f1} - \mathbf{C}_{f2} \mathbf{V}_r \mathbf{I}_{f2}$$

11. Carry out the magnitude deconvolution given by (Eq. 3.14)

$$\mathbf{E}_r = [\, abs\{\mathbf{C}_r\}]^{-1}\, abs\{\mathbf{V}_f\}.$$

Rearrange $abs\{\mathbf{E}_r\}$ into a column matrix $\mathbf{E}_s$.

12. Compute the autocorrelation $R(T_u)$ using (Eq. 3.6) in which E_{sk} are the elements of $\mathbf{E}_s$.

$$R(T_u) = 1/N \sum_{1}^{N} |E_{sk}|^2 e^{j2\pi(k-1)/N}$$

and the mean velocity using the phase of $R(T_u)$

$$\hat{v} = (v_a/\pi)\ arg\{R(T_u)\}; \qquad v_a = \lambda/(4T_u).$$

13. Form a NxN diagonal matrix $\mathbf{E}_a$ such that $diag(\mathbf{E}_a) = \mathbf{E}_s$.

14. Modify $\mathbf{E}_a$ by replacing first q and last (q-1) elements of the diagonal by the elements $(q+1)^{th}$ and $(N-q+1)^{th}$ elements, respectively, to get $\mathbf{E}_a^m$.

15. Determine the region of $\hat{v}$, and form the column matrix $diag(\mathbf{I}_v)$ (Eq. 3.19).

16. Compute the corrected spectrum, $\mathbf{E}_a^c$, using Eq. 3.16.

$$\mathbf{E}_a^c = \mathbf{E}_a\ \mathbf{I}_1 + \mathbf{E}_a^m\ \mathbf{I}_2\ \mathbf{I}_v\ \mathbf{Z}$$

where the matrices $\mathbf{I}_1$, $\mathbf{I}_2$, and $\mathbf{Z}$ are pre-computed and are input to the algorithm. (See Eqs.3. 17 to 3.20 for details of the matrices.)

17. Re-compute autocorrelation $R(T_u)$ using elements of $\mathbf{E}_a^c$ and then the bias corrected mean velocity from the phase of $R(T_u)$. The mean signal power is also computed from this spectrum.

18. Compute the extent of the residual spectrum to be deleted centered on the value of estimated velocity, $\hat{v}$. The extent to be retained is $\hat{v}\pm 2v_a/(n_1+n_2)$ in the velocity scale $0 \rightarrow -v_a \rightarrow v_a \rightarrow 0$ (cyclic).

19. Delete the residual coefficients and estimate the spectrum width using Eq. 6.37 of Doviak and Zrnic, 1993. Note that the $R(0)$ and $R(T_u)$ used in the expression for width must be calculated from the spectral coefficients after truncation, and not from the signal power and $R(T_u)$ computed earlier in Step 17.

20. Output the estimated spectral parameters, signal power, mean velocity, and width.

21. Go to the next data set (next gate).

========== end ==========

Note:

(a) The matrices $\mathbf{I}_{f1}$, $\mathbf{I}_{f2}$, $\mathbf{C}_{f1}$, $\mathbf{C}_{f2}$, $\mathbf{I}_1$, $\mathbf{I}_2$, $\mathbf{Z}$, and the magnitude deconvolution matrix, $[abs\{\mathbf{C}_r\}]^{-1}$, are to be computed only once and can be stored for use with each data set. If the clutter filter width is changed from one data set to the next, then we need to re-compute the matrices $\mathbf{I}_1$ and $\mathbf{I}_2$.

(b) In Step 16, all the matrices are diagonal matrices; hence, it is element by element multiplication of the diagonal elements. Therefore, in programming this step, it is simpler to represent all matrices as columns and use an element by element multiplication operator (dot operation).

4. Performance summary of staggered PRT algorithm.

So far, we have delineated a new spectral domain approach to processing the staggered PRT radar returns and have demonstrated the remarkable performance of the algorithm in effective clutter filtering with no velocity drop-out regions in the unambiguous velocity interval and improved spectral moment estimates. The results presented are for some specific choice of parameters. In the process of evaluating the suitability of the staggered PRT technique to WSR-88D, the parameters required may be different, and it is necessary to evaluate the performance of the algorithm for different choices of parameters and the limits of performance of the algorithm. Mainly, the parameters to be considered are κ, r_{a1}, v_a, w, $sd(v)$, $sd(w)$, M, d_t (dwell time, $d_t = (T_1+T_2)M/2$), etc. An overall $sd(v)$ performance of the algorithm for κ=2/3 and 3/4 is discussed in this section.

As mentioned earlier in the Introduction, the algorithm assumes that the staggered PRT time series samples are free from overlaid signals from second and higher order trips. The overlaid signals from the second or higher order trips severely degrade the performance of the algorithm. Therefore, it is important to select the PRTs, T_1 and T_2, so as to ensure no overlay. In the staggered PRT scheme using the pulse pair algorithm to compute the velocity, T_1 and T_2 are constrained by the unambiguous range and the desired accuracy in estimates. For the present

algorithm using the spectrum reconstruction procedure, an additional consideration enters; it is important to keep the ratio of available samples to the total number of samples (including the inserted zeros), $2/(n_1+n_2)=M/N$, as large as possible. The error in the reconstructed spectrum increases with decreasing M/N ratio. To keep the $sd(v)$ small, we also have to nearly satisfy criterion (3.5). It may be noted that all the results of the simulations for κ=2/3 are calculated using the number of staggered PRT samples, M=64; if the number of samples are different, the estimate variances also will also differ correspondingly. Therefore, in comparing the performance of the staggered PRT scheme with different stagger ratios, κ, it is more realistic to keep the dwell time, d_t, same (to have equal angular resolution) rather than the number of samples, M. Further, the most important restriction is that no overlay is allowed (the algorithm cannot separate overlaid echoes), which means that the scheme can be used only when no returns are expected from ranges beyond r_{a1}. The overall $sd(v)$ performance of the staggered PRT algorithm for the approximate WSR-88D dwell time of 42 ms, and two values of κ (2/3 and 3/4) are summarized in Figs. 4.1 and 4.2. These figures show $sd(v)$ as a function of w and v_a. Figs. 4.3 and 4.4 show the same set of data as in Figs. 4.1 and 4.2, but the $sd(v)$ is plotted as a function of normalized width, $(n_1+n_2)w/2v_a$. This shows that the $sd(v)$ variation is nearly the same as a function of normalized width and can be approximated to a single curve for all κ values. Note the multiplication factor (n_1+n_2) included in the normalization. There is a small spread of the curves because they are simulation results. For the same dwell times, all the curves nearly merge into one because the equivalent independent samples in a given dwell time is about the same. The results of simulation with constant d_t are presented in the 2-D shaded plots for the parameters of interest to WSR-88D because these are easier to read and interpret. The unambiguous range, r_{a1}, is also shown on the right hand side corresponding to the v_a shown on y-axis.

A large number of simulations were carried out to determine the standard error in the velocity estimate for different values of v_a (or T_u) and spectrum widths, for d_t=42ms. The $sd(v)$ values grater than 5 m s^{-1} are limited to 5 m s^{-1} for plotting. The actual values of $sd(v)$ obtained from simulations are shown in Tables 4.1 and 4.2. Each value of $sd(v)$ is obtained from 800 simulations (20 simulations at each of 40 different velocity values, spread uniformly

over $\pm 0.8 v_a$). It is seen that once criterion (3.5) is violated, the $sd(v)$ increases sharply because the reconstruction of the spectrum becomes inaccurate. This limit is approximately 0.225 for $\{(n_1+n_2)w/2v_a\}$ (see Fig. 4.3, 4.4). In all these plots, there is no clutter filtering implemented; therefore, the $sd(v)$ is only due to the spectrum reconstruction procedure (i.e., no ground clutter). With the ground clutter filtering, the $sd(v)$ is larger because there is always some residual clutter which can be considered as noise. This degradation can be minimized by selecting appropriate clutter filter width which optimizes the velocity recovery.

The performance with respect to the clutter filtering is presented in the next three figures for κ=2/3, 3/4, and 4/5 for a selected set of parameters. Figs. 4.5, 4.6, and 4.7 show plots of estimated velocity versus the input velocity with dwell times and r_{a1} same for all three schemes. For convenience of comparison, the estimated velocities are shown on the same plot with a vertical shift for different CSR values. Only the lowest set (CSR=30 dB) has the correct vertical velocity scale; the rest of the plots are shifted by $v_a/2$ for each 5 dB increase in CSR. Because r_{a1} and dwell time is kept the same, the unambiguous velocity and number of samples are different for the three figures. Also note that the vertical scales are different for the three figures. The velocity recovery is good to about CSR=40 dB in the case of κ=2/3 but has many outliers for larger CSR. The same can be said for other κ values, but the standard error is a little larger. These seven figures reasonably summarize the performance of the staggered PRT scheme with the new clutter filtering algorithm. Using these figures, we shall try to evaluate the usefulness of the staggered PRT scheme to the WSR-88D.

Although larger stagger ratios provide larger unambiguous range and/or velocity (Fig.4.8), we can only use them to increase the unambiguous velocity (at the expense of an increase in the $sd(v)$) because the unambiguous range is restricted by the requirement that no overlaid signal is allowed. Further, $2v_a/(n_1+n_2)$ must be large enough (at least 3.5 times the spectrum width) to be able to recover velocities of signals with spectrum widths up to about 6 m s^{-1} (Eq. 3.5). These two restrictions must be kept in mind while selecting the parameters for the staggered PRT scheme.

5. Alternatives to the WSR-88D scan strategy.

The WSR-88D has pre-programmed scan strategies, designated by vcp-11, vcp-21, etc., and each volume coverage pattern (vcp) has a fixed set of elevation scans with pre-set parameters. In the lowest elevation (0.5°), there are two scans, one with a long PRT (~3 ms) to get an unambiguous display of reflectivity to 460 km and a second (Doppler) scan with a short PRT (selectable among five pre-set PRTs) to estimate velocity. The Doppler scan is generally plagued with multiple trip overlay and loss of velocity information. The same procedure is repeated for the next elevation, 1.45°. For 2.4° to 6.2° elevation scans, the long and short PRTs are used in alternate radials and are labeled as batch mode. In Fig. 5.1 is a range-height diagram for the WSR-88D elevation scans. It shows the ray paths in the range-height space taking into consideration the Earth's curvature. As per the NEXRAD volume coverage requirement specifications, height coverage is required up to 70,000 ft (21.12 km), but most storms do not extend to that height. If we assume that most storms extend to a height of 18 km or less, the clear range requirement for each elevation scan can be read out from the figure. For the intermediate elevation scans (2.4° to 6.2°), the range requirement varies from 303 km to 154 km.

As a result of our three year study, two new schemes have emerged as candidates for the resolution of range and velocity ambiguity in WSR-88D, in addition to the present WSR-88D coding scheme (e.g., batch mode). They are the staggered PRT scheme and the SZ phase coding scheme. All schemes have the capability to resolve ambiguities in range and velocity but with certain limitations. Therefore, we need to make compromises in selecting the scan parameters and the scheme. *In making these compromises we shall assume that any changes made in the scan strategy and the scheme should improve the performance without giving up on the present WSR-88D performance.* First, we examine the range requirements, scan rates, the number of samples available, etc. and then work within these restrictions to select one or the other scheme with possible PRTs and scan rates, taking into consideration the quality of the spectral moment estimates, the velocity estimates in particular.

It is significant that we come across spectrum overlap in the staggered PRT scheme as well as in the SZ phase coding scheme, but the way in which the spectrum overlap affects the $sd(v)$ is different in the two schemes. In the staggered PRT scheme, there are five complex

weighted replicas of the spectrum within the $\pm v_a$ interval (for κ=2/3), and the magnitude deconvolution produces residuals due to the spectrum overlap which contributes to the $sd(v)$, if not to the bias error. Similarly, in the case of SZ(8/64) phase coding, we have eight complex weighted replicas in the $\pm v_{ap}$ (subscript 'p' is used to distinguish the two unambiguous velocities) interval (which is generally smaller than that of the staggered PRT), and after notch filtering and cohering, the original signal and six side bands are present in the spectrum from which velocity is computed. For the same $\pm v_a$ interval and the spectrum width (of the weaker signal in the case of SZ phase coding), the spectrum overlap is much larger in the case of phase coding than in the staggered PRT with κ=2/3, but the contribution to the $sd(v)$ is much less because velocity is computed from the complex spectrum before the magnitude deconvolution. The overlap appears to produce some perturbations in the spectrum (which can be treated as noise) which contributes to the $sd(v)$. The magnitude deconvolution in the phase coding scheme is used only for spectrum width estimation. Further, the above mentioned $sd(v)$ is for the weaker signal, but the stronger signal velocity is always recovered. The weaker signal velocity is recovered if the overlay power ratio is within about -40dB $<p_1/p_2<$40 dB. Clutter filtering is also possible with the SZ phase coding scheme up to about CSR=50 dB with the spectral domain filtering. This is significantly better than what we can achieve with the staggered PRT scheme. There is a small bias in the velocity whenever the velocity is close to the zero Doppler, just as in the case of the staggered PRT scheme. This bias can also be nearly compensated by the same technique as described for the staggered PRT bias correction scheme. That is, instead of simply deleting the first q and the last (q-1) coefficients centered on the zero Doppler, replace the coefficients with $(q+1)^{th}$ and $(N-q+1)^{th}$ element values, respectively, which will remove the bias to a large extent. Although the SZ coding scheme appears to perform better in terms of the $sd(v)$ compared to the staggered PRT, it is more complex to implement, both in hardware and processing software. The SZ coding scheme needs a phase shifter and the DFT computation several times in the processing, whereas the staggered PRT scheme requires only a change in the PRT and a one time DFT computation. One additional advantage of the SZ coding scheme is that the two overlaid signals need not necessarily be from the 1st and 2nd trips but can be any two trips whenever there are multiple trip ranges covered by the selected

PRT. Even for three trip overlaid signal, a limited velocity recovery (of the two stronger signals of the three) can be devised with reasonable success. The present staggered PRT algorithm does not allow overlaid signal; hence, T_1 must be chosen corresponding to the maximum unambiguous range. With these comparative remarks, let us try to compare the three schemes for each elevation scan of the WSR-88D.

Table 5.1a gives the vcp-11 scan parameters of the WSR-88D, and the PRT values are listed in Table 5.1b. From the number of samples and the PRT, the dwell time per radial can be computed, and it varies between 53 ms and 42 ms for different elevations. The exact dwell times for each elevation are listed in Table.5.1c along with the standard errors in the reflectivity, velocity, and the spectrum width estimates obtained from simulation using the default PRT values. This gives us the number of staggered PRT or the SZ phase coded samples available for processing signals from each range gate, keeping the dwell time same as that of the WSR-88D. Thus, M=64 used in most of the computations seems reasonably close to that available in practice if the PRT is about 1 ms for lower elevation scans. The possible staggered PRT parameters for each elevation scan of WSR-88D is presented in Table 5.2. In generating this table, it is assumed that there is only one staggered PRT scan at each elevation, keeping the total scan time for each elevation the same. The number of samples M is calculated for the WSR-88D dwell time and is rounded off to the nearest even number. In practice, we can get about 30 percent more samples using the sample overlap scheme explained in Part-2 of this report (Sachidananda et. al., 1998). The last column is the approximate value of signal spectrum width for which $sd(v)$ is within a limit of about 2 m s^{-1}. The values are approximate and are arrived at based on the simulation results with M=64. Therefore, for lower elevations, the limit of width is less than given in the last column, and for elevations higher than 6.2°, it is larger than the value given in the last column. An examination of Table 5.2 indicates that staggered PRT is good for elevations 5.25° and above. For lower elevations, the unambiguous velocity is not sufficiently large to enable recovery of the velocity accurately for widths up to at least 5 m s^{-1}.

Now, compare the performance of the SZ(8/64) coding scheme to that of the staggered PRT scheme for elevation 5.25°. With a PRT of 0.59 ms for the SZ coding scheme, we get

$2r_a$=177km, with the first trip interval being 88.5km. The stronger trip signal parameters are completely recovered, and the weaker trip signal parameters are recovered for overlaid power ratios less than 40 dB and for widths up to about 6 m s^{-1}. The unambiguous velocity is also 42.37 m s^{-1}, the same as that for the staggered PRT. Therefore, the performance is certainly better than that of the staggered PRT scheme, but with more complex signal processing. The SZ coding can work well with v_a=33 m s^{-1} for 3.35° elevation, giving a range coverage up to 224 km with only a 2 trip overlay. For 2.4° elevation, one can still select a PRT of 0.92 ms with a full range of 276 km and get a reasonable recovery of the weaker trip signal. There may be some loss of the velocity information of the weaker signal whenever the stronger trip signal is wide (> about 4 m s^{-1}).

For the lowest two elevations, there is no escape from multiple trip overlay. Therefore, the long PRT scan becomes imperative if we were to retain the clear reflectivity over the full range for these two scans. The Doppler scans can be SZ phase coded and at least recover velocity in some of the regions which otherwise would be lost in the present WSR-88D coding schemes. The stronger trip signal velocity is mostly recovered, but the weaker signal velocity recovery is dependent on its strength and the number of echoes overlaid.

Table 5.3 is a possible modification to the WSR-88D scan strategy. For the first two elevations, the long PRT scan is retained for the reflectivity. The Doppler scan is replaced by the SZ phase coded transmission. For the intermediate elevations from 2.4° to 4.3°, the batch mode is replaced by SZ coded transmission. The possible PRT selections for each elevation are indicated in the table. For the elevations 5.25° and above, the staggered PRT with appropriate selection of the T_1 and T_2 is advantageous because it allows much larger unambiguous velocity for the required unambiguous range which can eliminate the need for dealiasing the velocity fields.

6. Suggestions for identifying high variance data estimates.

The base data collected by the radar must be reasonably accurate before it can be used for meteorological interpretations. There are always bad data or high variance data which do not represent the actual spectral moments because of several limitations of the radar. For example,

one of the most common reasons for bad velocity data is the 2nd and higher order trip overlay. In the WSR-88D, these estimates are identified as unusable. With the introduction of the SZ phase coding and/or staggered PRT techniques for the mitigation of the range and velocity ambiguity problem, we can recover major regions of the velocity data, but these techniques, too, have their limitations. The accuracy of the spectral moment estimates is affected by the spectrum width, clutter-to-signal ratio (CSR), overlaid power, signal-to-noise ratio (SNR), etc. In the absence of a way to recover spectral moments in these special situations, it becomes necessary to at least identify these data as unusable so that wrong conclusions/interpretations of the meteorological phenomenon are avoided. In this section, we shall examine the ways of censoring the high variance/erroneous base data for SZ phase coding and the staggered PRT schemes.

There are two approaches that can be considered: (1) rejection criterion based on one or combination of several parameters estimated for each range gate, and (2) censoring criteria based on the spatial continuity/variance of the data. The first approach can be implemented in almost real time because the criterion uses a single set of samples for each gate, and the rejection criterion can be built into the spectral moment estimation algorithm. The second approach is best implemented off line after the data is collected. It can also be implemented in almost quasi-real time if we confine our spatial variance computations to a single radial of data or data from a few radials in azimuth direction. The second approach is based on the high degree of spatial and temporal continuity of the weather data.

We require different criteria for the staggered PRT and the SZ phase coding schemes, and these are discussed separately in the paragraphs that follow. The discussion here is mainly based on the extensive simulations carried out for the range and velocity ambiguity resolution in WSR-88D using these two schemes.

6.1. The data censoring for the staggered PRT scheme.

In order to arrive at proper criteria for data censoring, we shall first examine the limitations of the staggered PRT scheme and the conditions under which the scheme fails to recover the spectral moments accurately. First of all, the present staggered PRT scheme does

not have the capability to resolve the overlaid signal, and therefore, it can be used only if no echoes are expected beyond the time T_1 after the transmission of the pulse. But in practice, this cannot be ensured 100 percent of the time, and the present WSR-88D processing techniques cannot give this guarantee. Furthermore, it would not be an optimum choice of PRTs if we try to ensure it. For example, we can choose a maximum unambiguous range for a given elevation scan by assuming that most storms (but not all) do not extend beyond a height of about 18 to 20 km above ground. One could even reduce this height and allow some weaker signal overlay to gain on the unambiguous velocity interval. This is possible because an overlaid signal 10 dB below the 1st trip signal strength does not produce appreciable error in the velocity estimate; hence, it can be tolerated. But there must be a way of determining the overlaid signal power ratio so that if the overlaid signal is more than a predetermined threshold value, one can discard the velocity estimate.

The second limitation is the maximum clutter power that can be effectively filtered; the effectiveness is being gauged mainly by the accuracy of the velocity estimate. (One can also include the accuracy criteria on other spectral moments.) Here, the relative clutter power level or the CSR is of importance and not the absolute clutter power. There is an upper limit for the CSR beyond which the velocity estimate is inaccurate. The limit is a strong function of the clutter spectrum width and the clutter filter width used in the processing and a weaker function of the signal spectrum width. For example, for T_u = 0.5 ms, κ = 2/3, w_c = 0.35 m s^{-1}, and w_f = 8 m s^{-1}, the velocity estimate is good up to CSR = 40 dB, for larger CSR outliers begin to appear, especially in the region where clutter and signal spectra overlap (i.e., around ± 20 and ± 40 m s^{-1}). The variance of the velocity estimate also increases around these velocities with increased spectrum width of the signal. This limit was observed in a simulation study with the input parameters mentioned above. For other selection of parameters, we need to determine appropriate limits for the CSR and spectrum width beyond which the data can be censored. The SNR also affects the variance of the estimates. Thus, the parameters to be watched are the CSR, SNR, overlay power ratio, spectrum width of the signal, spectrum width of the clutter, and the clutter filter width.

Having identified the parameters and their limits to censor the data, we must have some

means of determining whether these limits have been crossed. Generally, the receiver noise floor is known, and therefore, SNR can be determined from the received signal power. For accurate spectral moments, the SNR required is more than 10 dB. Similarly, the distribution of the ground clutter in range, azimuth, and elevation, as well as its statistics in terms of the power level and spectrum width can be determined from a clear weather scan data. This information can be stored in a data base and can be used by the decoding algorithm to estimate CSR and derive appropriate limits for data censoring. Note that this information is also needed for deciding the clutter filter width to be used in the algorithm.

It is observed that a large signal spectrum width also can lead to a high variance velocity estimate, but it is difficult to decide definitely on a upper limit for the spectrum width estimate. The simulation study indicated that the large spectrum width does not necessarily indicate a bad velocity estimate always, and visa versa. This is because the spectrum width estimate itself is generally very noisy. Therefore, making a decision on the accuracy of the velocity estimate based on the width estimate is highly undesirable.

The only parameter that cannot be estimated easily in the present staggered PRT scheme is the overlay power ratio. If the long PRT (T_2) is large enough to include all the echoes but not the short PRT (T_1), then we can devise ways to estimate the overlay power ratio. But if the overlay is from two range gates, i.e., there are returns with delay time greater than T_2, then estimating overlay power ratio is difficult. For the second case with two gate overlay, there is no way of estimating the overlay power unless we employ a long PRT scan, as in the lowest two elevation scans of the WSR-88D, although an overlay power of -10 dB with respect to the signal can be tolerated.

6.2. Data censoring for the SZ coding scheme.

The SZ phase coding scheme is basically a method to resolve two overlaid echoes and estimate their spectral moments, thus doubling the unambiguous range for a given PRT or doubling the unambiguous velocity for the same unambiguous range by halving the PRT. In both cases, it is important to make sure that only two signals are overlaid. It is also possible to decode multiple trip overlay but with greatly reduced capabilities. The method works best for

two trip overlay. There is, of course, a limit on the ratio of overlaid powers, SNR of the weaker signal, maximum allowable random phase error in the phase shifter and the radar system transmit-receive path, spectrum width of the stronger of the two overlaid signals, number of samples available for each range gate, etc. These parameters determine the standard error in the spectral moment estimates. In general, velocity estimate is affected the most, and the other two parameters, signal power and spectrum width estimates, are affected to a lesser extent. Therefore, the allowable limits on the above listed parameters is best derived considering an upper allowable limit on the $sd(v)$. A standard error of 1 m s^{-1} is generally accepted in the velocity and the spectrum width estimates, and a standard error of about 2 dB (1.2dB for the lowest two elevation scans) is tolerated in the reflectivity estimate in the present WSR-88D. This is for the uniform PRT transmission and no higher order trip overlay. But for the SZ phase coding scheme, the lowest achievable $sd(v)$ is slightly larger for the weaker signal, for the same set of signal parameters, because the stronger signal is not completely filtered out in the notch and cohere process. A small part of the stronger signal remains in the spectrum and is equivalent to noise, thus degrading the equivalent SNR. The residual stronger trip signal after notch and cohere is due to two reasons, 1) the random phase error in the phase shifter and the radar system does not allow 100 per cent cohering of the stronger signal, and 2) the notch filter does not remove all the overlaid signal power which is cohered. Because of these reasons, for w_1 = 4 m s^{-1} and w_2 = 4 m s^{-1} (spectrum widths of the two overlaid signals), the lowest achievable $sd(v)$ is about 1.5 m s^{-1} for the practical random phase error of 0.2° in the radar system. The upper limit ratio of the overlaid powers is about 40 dB. For larger p_1/p_2 ratios, the velocity estimate can be censored. Fortunately, many of the parameters required for data censoring can be estimated or measured. For example, the phase shifter random error can be evaluated a priori from measurements. The noise floor of the receiver is also known so that from the received signal power, the SNR can be determined. The SNR of the weaker signal, which is the deciding criterion, can be calculated after the weaker signal power is estimated. The p_1/p_2 ratio also can be accurately estimated up to about 50dB for median spectrum widths. The censoring limits for the p_1/p_2 ratio is a function of the spectrum width of the stronger of the two overlaid signals, which can also be accurately estimated. The limit can be obtained from

Fig. 5.6 of Sachidananda et. al, 1998. The velocity estimate is censored for p_1/p_2 >40dB; w_1<4 m s^{-1}. For larger widths the p_1/p_2 limit has to be set lower depending on the estimated value of w_1 . These censoring criteria can be incorporated in the decoding algorithm to automatically eliminate the high variance data.

6.3. Censoring data field based on spatial high variance.

It is well known that the spectral moment fields exhibit a high degree of spatial and temporal continuity. This fact can be effectively used for data censoring. This data censoring procedure is independent of the transmission scheme used and can be implemented in real time, quasi-real time, or off-line. For real time implementation, it would be best to base the decision on the spatial variance of the data along one radial at a time. In the off-line or quasi-real time implementation, one can use the 2-dimensional spatial variance.

One simple scheme could be to compute the gradient field by taking the difference between the successive gate parameters (reflectivity, velocity, and width). The outliers would produce sudden discontinuities (positive and negative spike pairs in the gradient). If there is a single isolated spike pair in the data field, it may also be possible to discard that particular data point and insert an interpolated value for that point. If there is a region with a noisy gradient field, then it is an indicator of low SNR or high CSR, and these regions can be censored. In the velocity field, if there is a discontinuity due to velocity folding, this would appear as a positive spike or a negative spike. The velocity discontinuity information is used at present in the velocity unfolding algorithm.

Generally, the velocity estimate gets corrupted by the noise, the overlay, or the clutter before the reflectivity is affected. The width estimate is inherently noisy and is not a good parameter to base the censoring decision on. Therefore, the velocity field is perhaps the best to work on, and if the velocity estimate for a gate or group of gates is found to be erroneous, the reflectivity and the spectrum width fields also can be censored for the same gates. All that is needed is a criterion or a limit on the maximum gradient above which the data is censored. It may be necessary to normalize the gradient with respect to the local mean value of the parameter being considered because of the large dynamic range of the parameters. The limits

for data censoring are best derived using the actual data; however, in the absence of actual radar data, we can use simulations to arrive at these limits.

6.4. Conclusions.

This brief discussion on censoring the high variance data is based mostly on the extensive simulation study carried out for the resolution of range and velocity ambiguity in WSR-88D using the staggered PRT and the SZ phase coding scheme. Each of these schemes have complex decoding algorithms which may fail under certain conditions of excessive clutter power, excessive overlaid power, large spectrum width, etc. We have identified the limitations under simulated conditions, but for actual implementation, one needs to try the methods on actual radar data and establish the validity of the results obtained from simulation study. Whereas the data censoring methods indicated for the staggered PRT and the SZ coding scheme should be implemented, one should also examine the use of spatial variance of the data field. This would allow us to recover velocities of the occasional outliers between good data by interpolation, and which can be incorporated as a part of the velocity unfolding algorithm.

-------oooo00000oooo-------

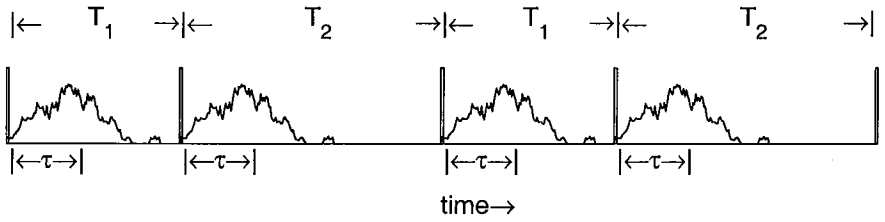

(a) Staggared PRT sampling scheme.

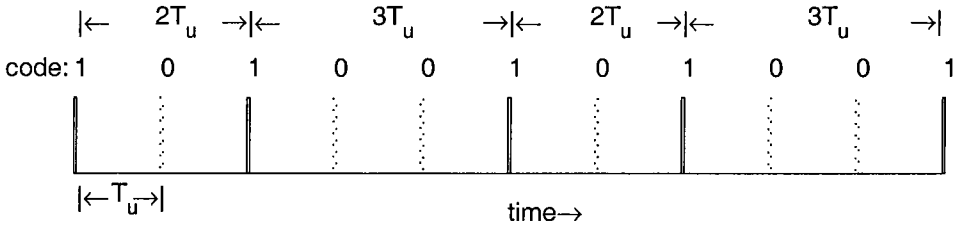

(b) Equivalent uniform PRT sampling, κ =2/3.

Fig. 2.1. The staggered PRT scheme. a) Transmit pulses and received echoes from a storm; τ is the range delay. b) The code and its relation to the staggered sequence.

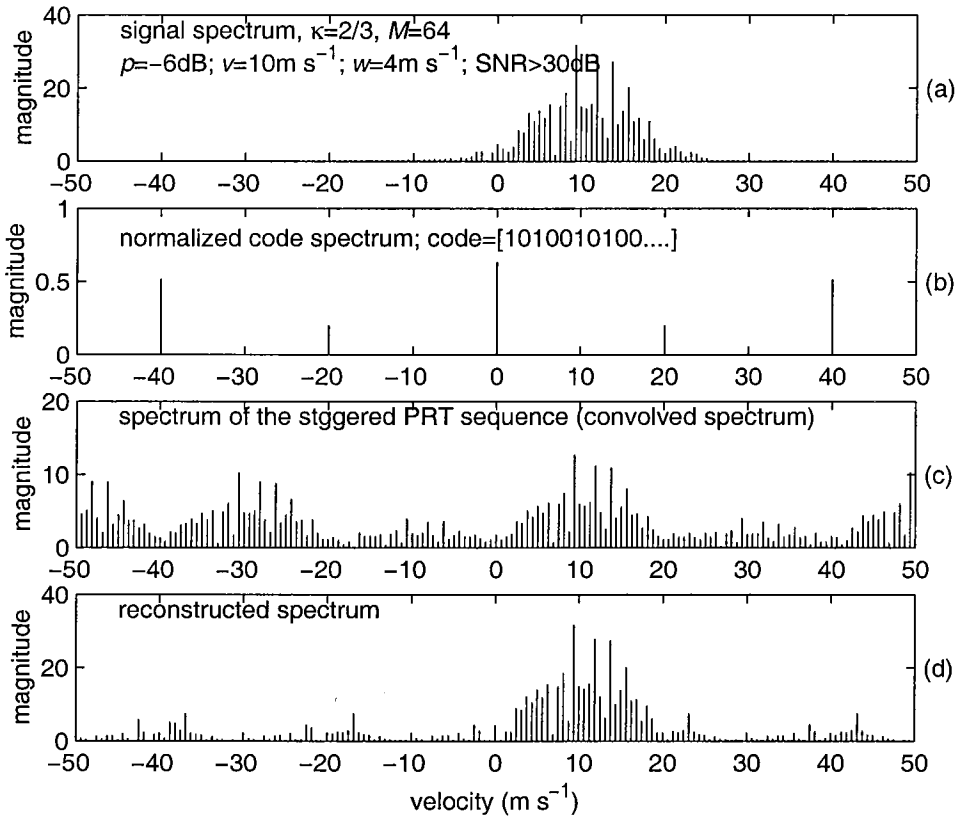

Fig. 3.1. An illustration of the magnitude deconvolution to reconstruct the signal spectrum from the staggered PRT samples.

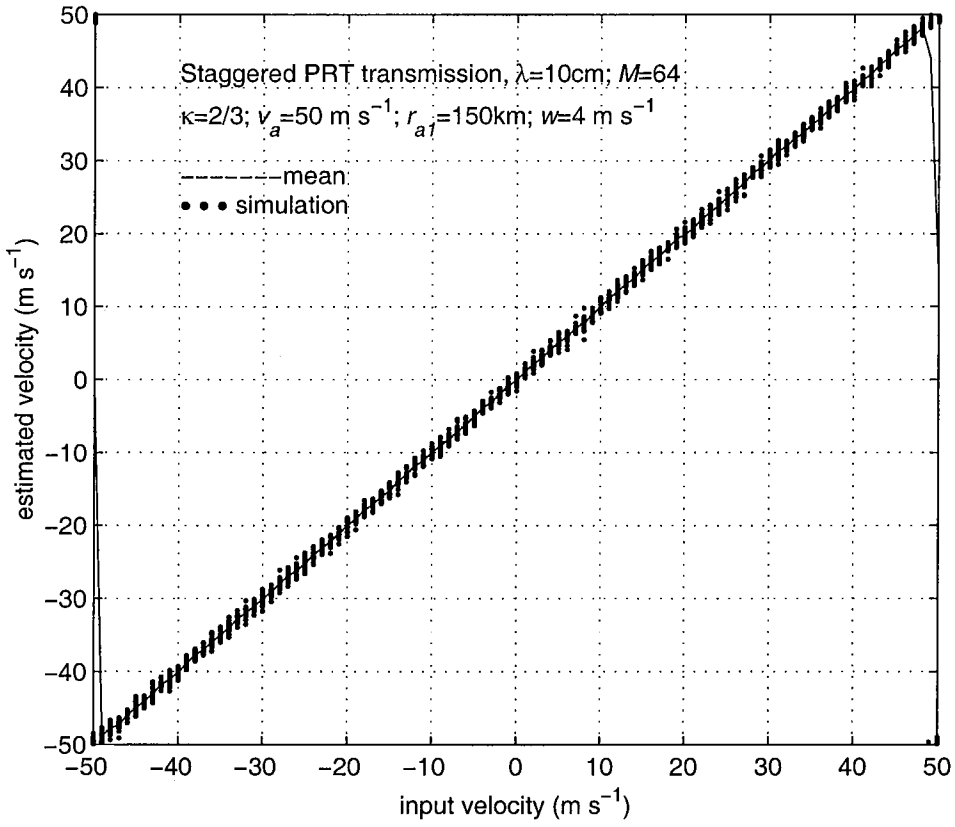

Fig. 3.2. Input velocity versus the estimated velocity using the magnitude deconvolution for κ=2/3. The clutter and window were not included in these simulations.

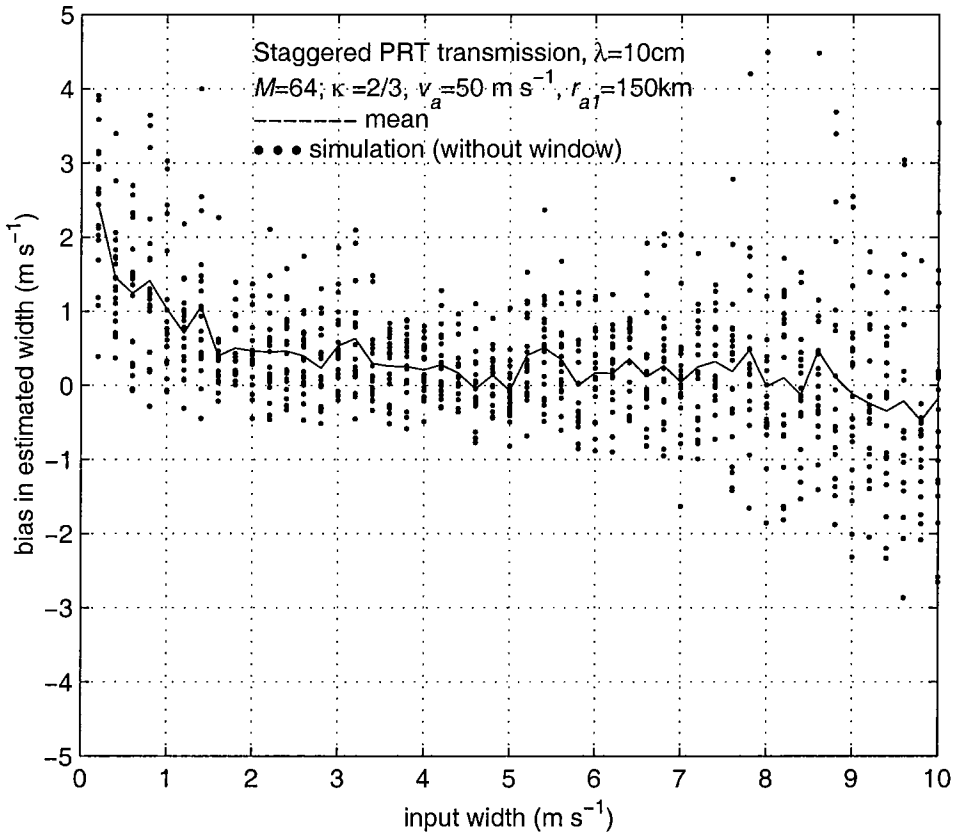

Fig. 3.3. Bias in the width estimate as a function of input width, without the window. The continuous curve is the mean value, and the dots are simulation points. The input velocities for simulation are spread uniformly over $\pm v_a$.

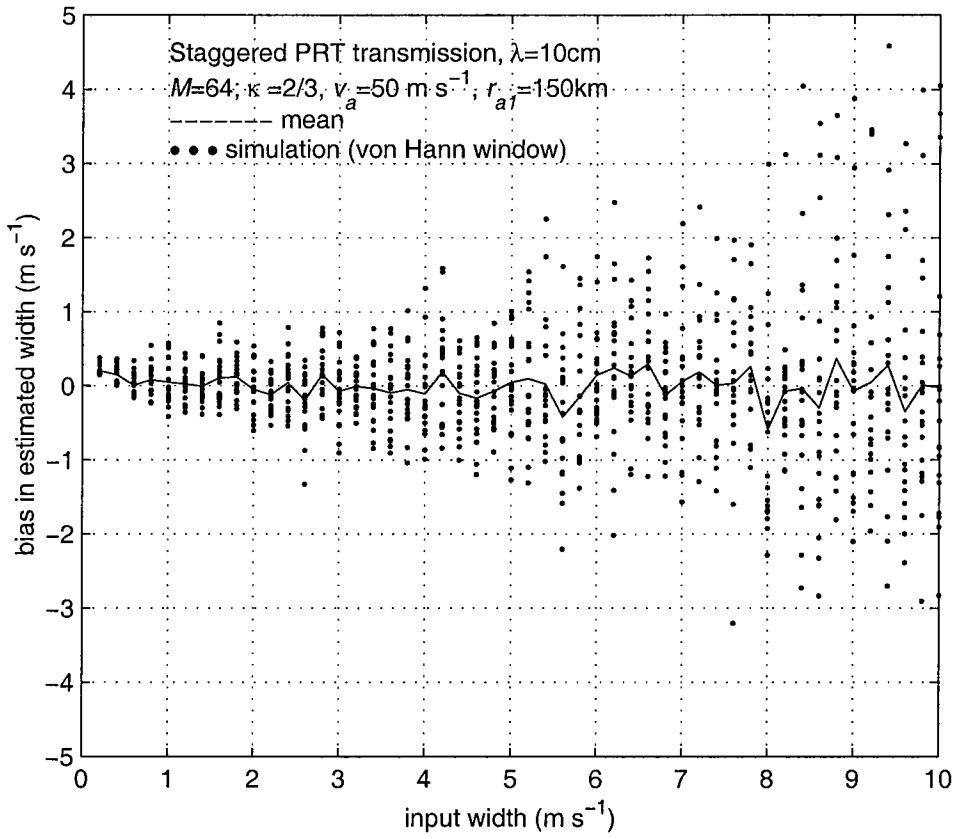

Fig. 3.4. Bias in the width estimate as a function of input width, with the von Hann window. The continuous curve is the mean value, and the dots are simulation points. The input velocities for simulation are spread uniformly over $\pm v_a$.

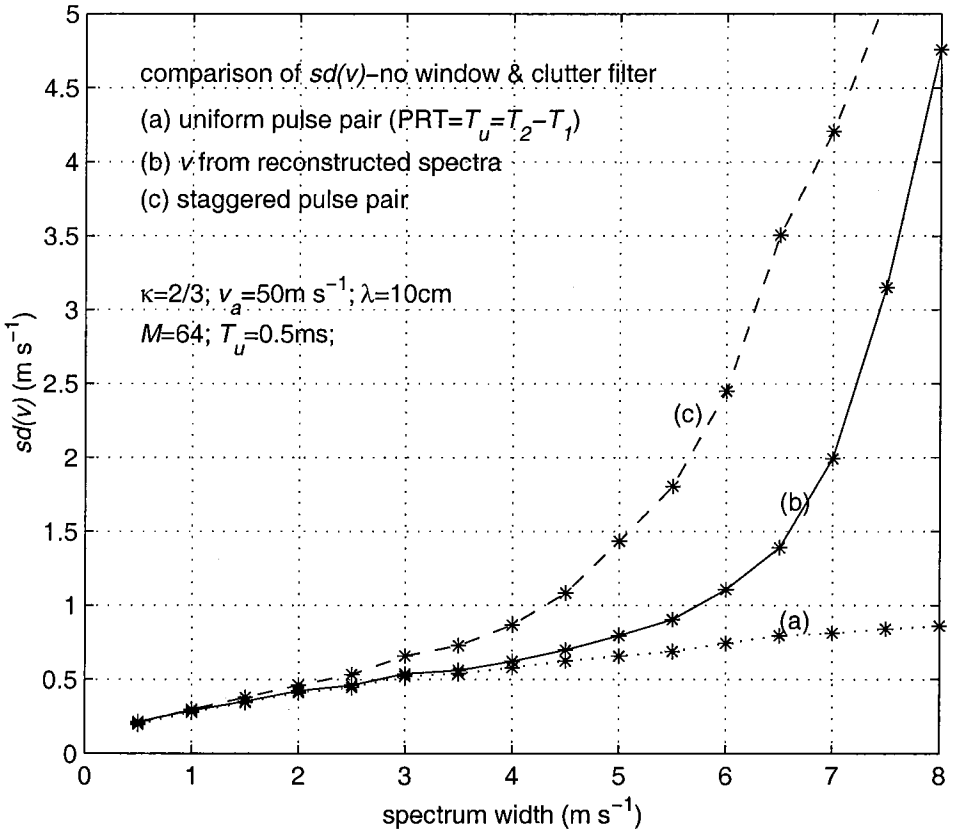

Fig. 3.5. Standard deviation of the error in the velocity estimate as a function of spectrum width of the signal (a) using complete time series samples, (b) using the reconstructed spectrum, and (c) using the ratio of $R(T_1)/R(T_2)$.

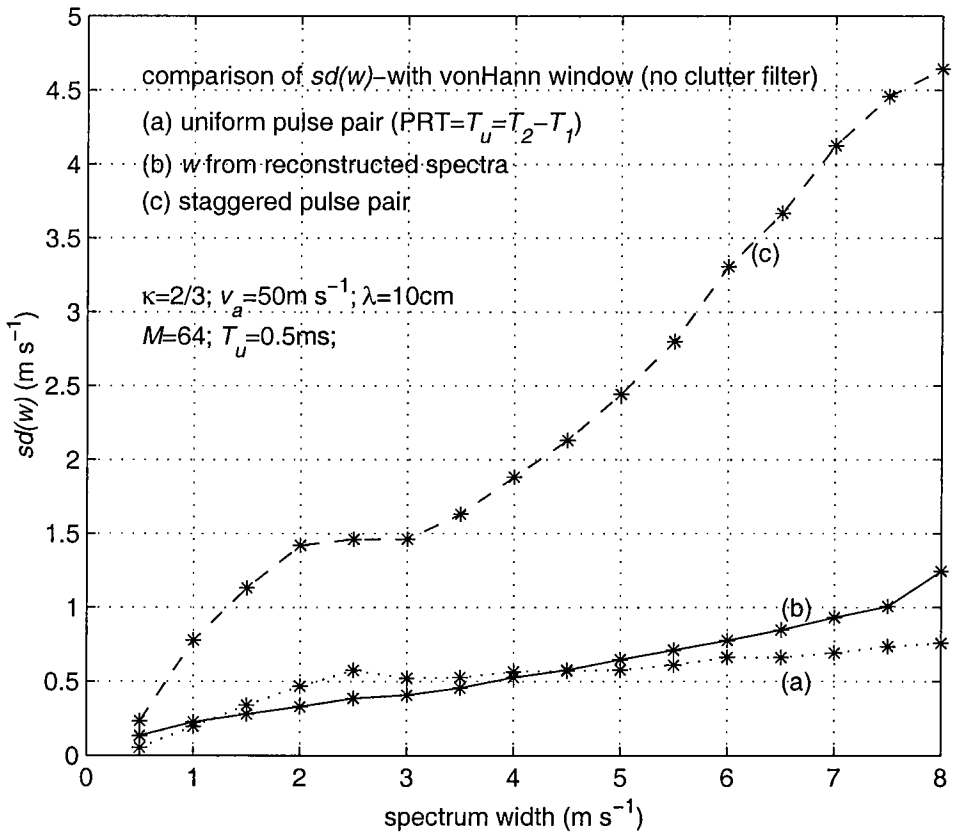

Fig. 3.6. Standard deviation of the error in the spectrum width estimate as a function of spectrum width of the signal (a) using complete time series samples, (b) using the reconstructed spectrum, and (c) using the staggered PRT samples.

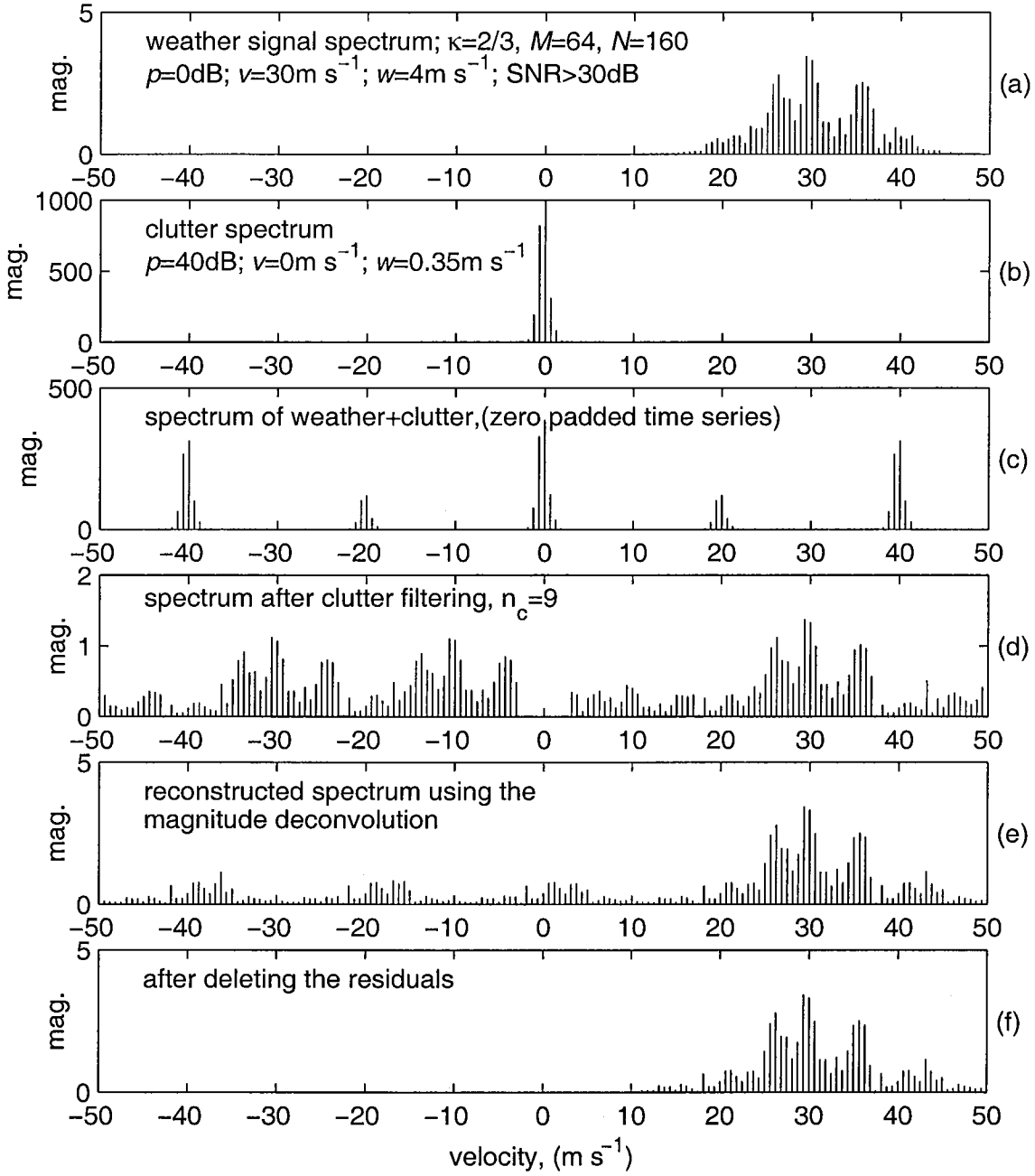

Fig. 3.7. An illustration of the clutter filtering procedure in the proposed algorithm.

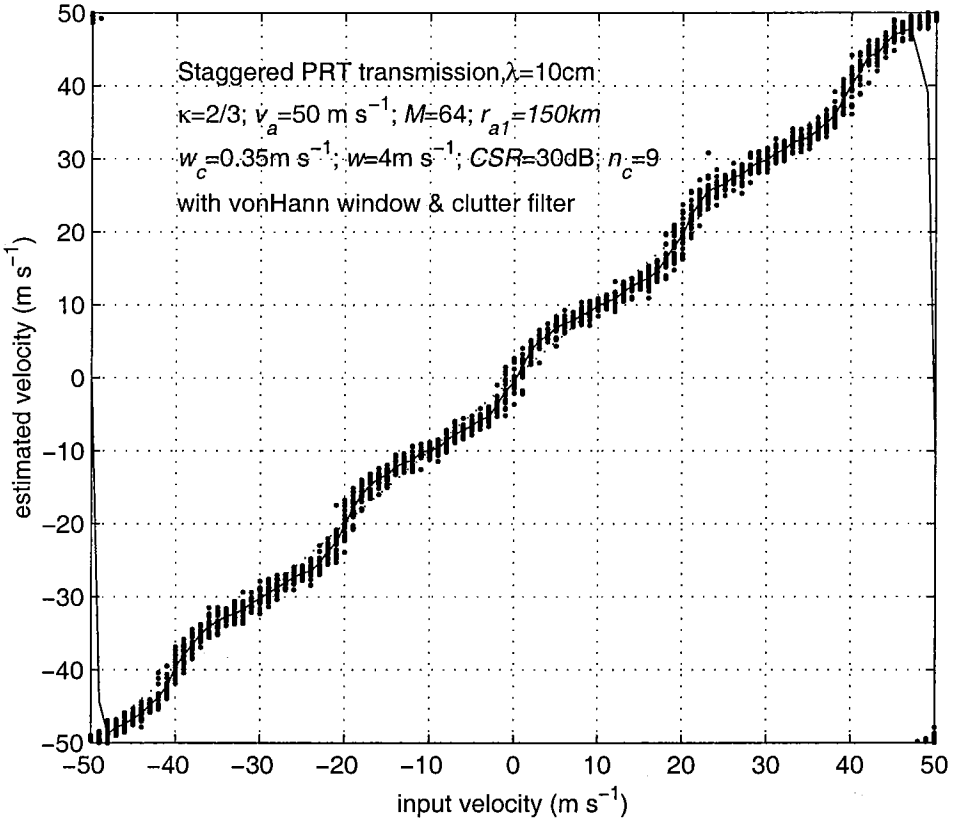

Fig. 3.8. Input velocity versus the estimated velocity using the proposed clutter filtering and spectral moment estimation algorithm. The parameters used in this simulation are indicated in the figure.

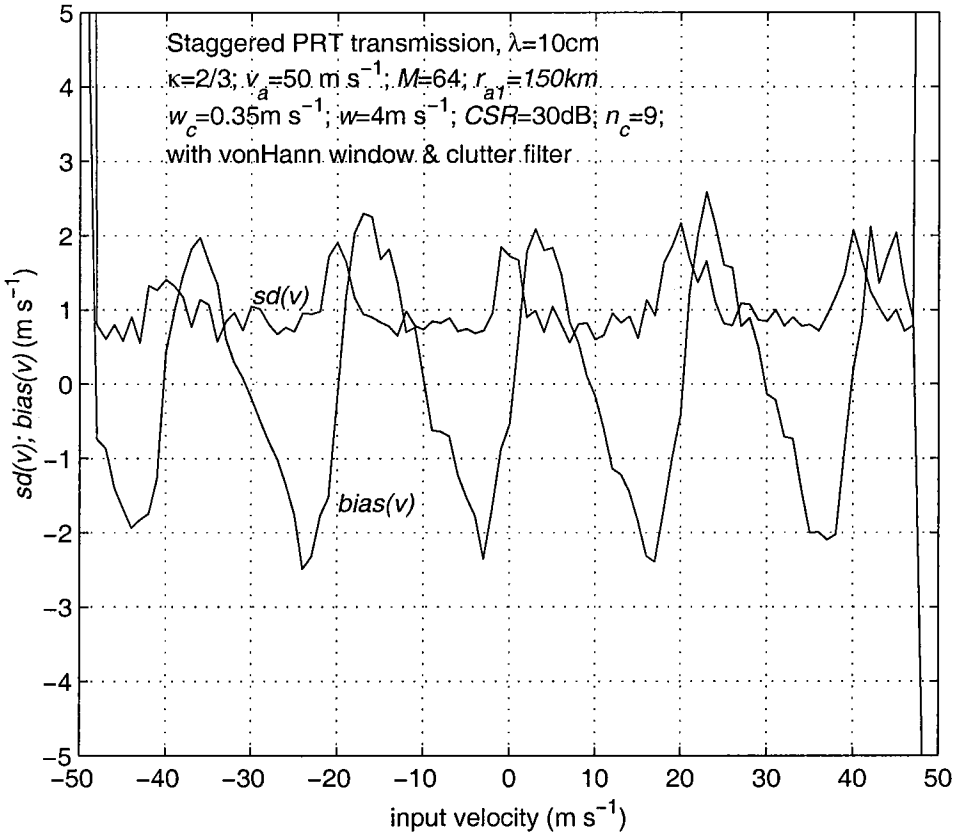

Fig. 3.9. Bias error in the velocity and the standard error in the velocity estimates using the proposed algorithm (κ=2/3). The simulation data is the same as that in Fig. 3.8.

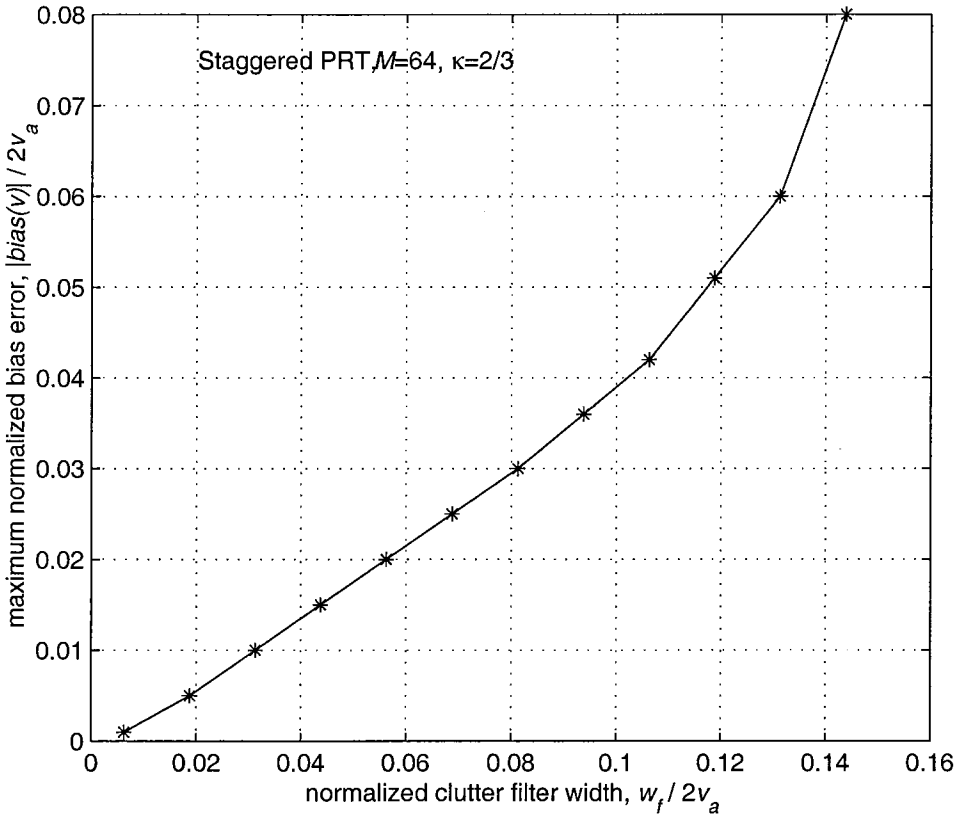

Fig. 3.10. The maximum normalized bias error in the velocity estimate as a function of normalized clutter filter width. The normalization is with respect to the unambiguous velocity interval, $2v_a$.

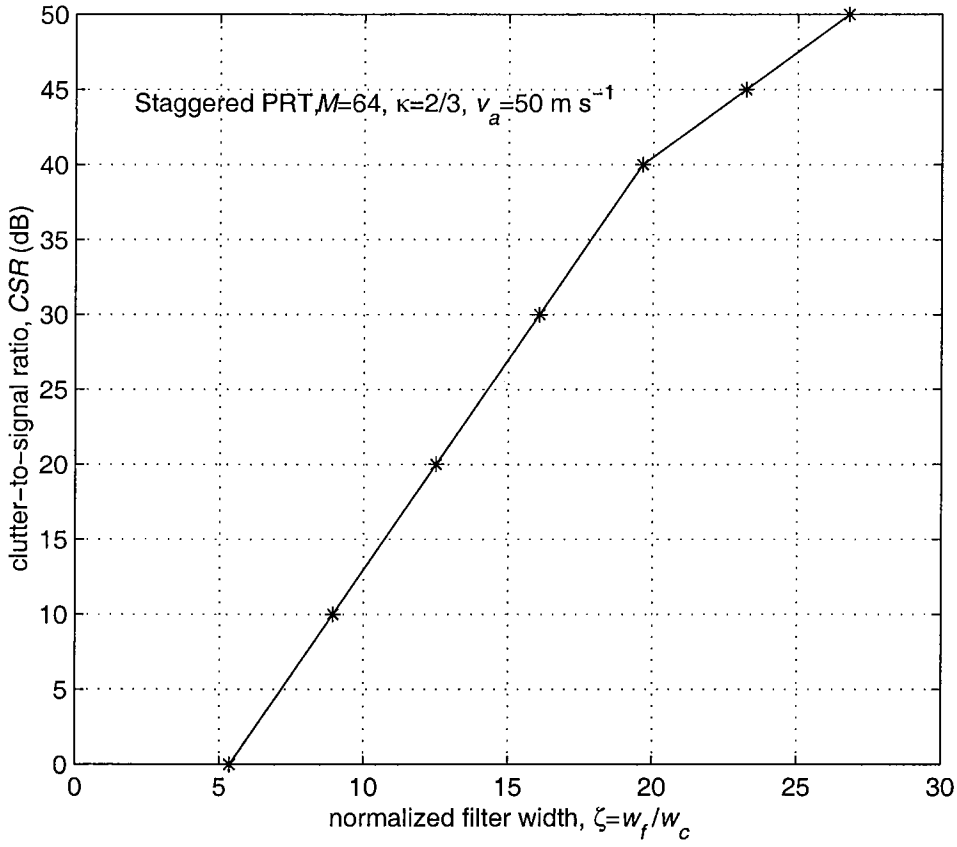

Fig. 3.11. The clutter-to-signal ratio (CSR) that can be filtered effectively versus the clutter filter width normalized to the clutter spectrum width.

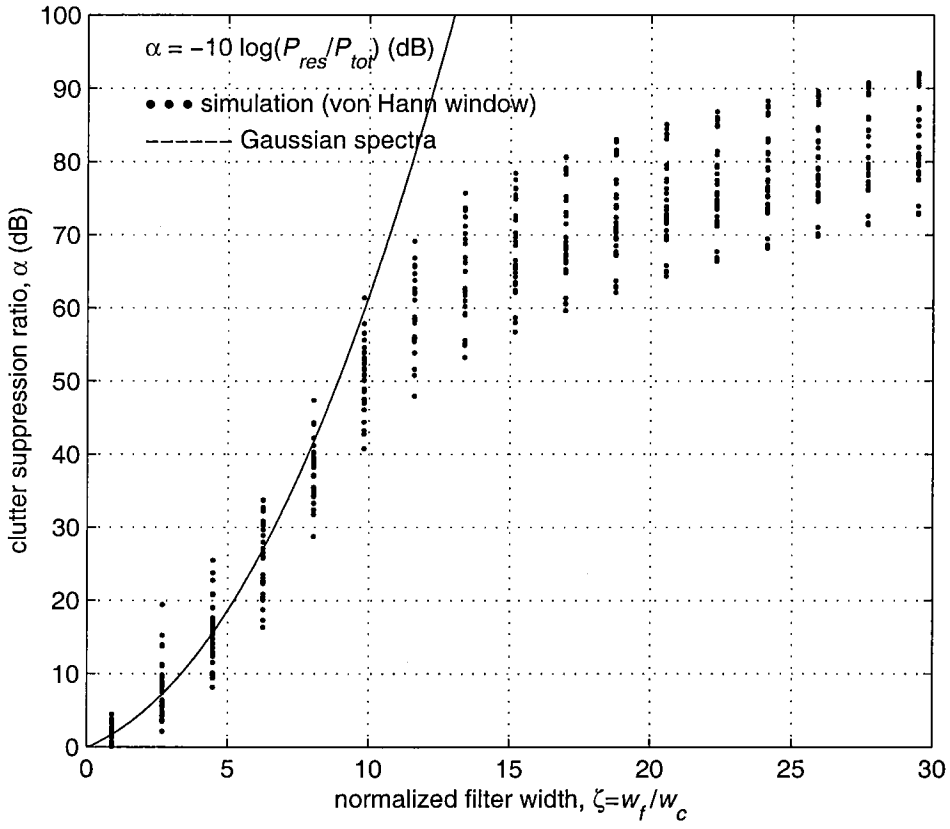

Fig. 3.12. The clutter suppression ratio as a function of the clutter filter width normalized with respect to the clutter spectrum width for Guassian spectra. The continuous curve is the theoretical for Gaussian spectra, and the dots are simulation points with the von Hann window.

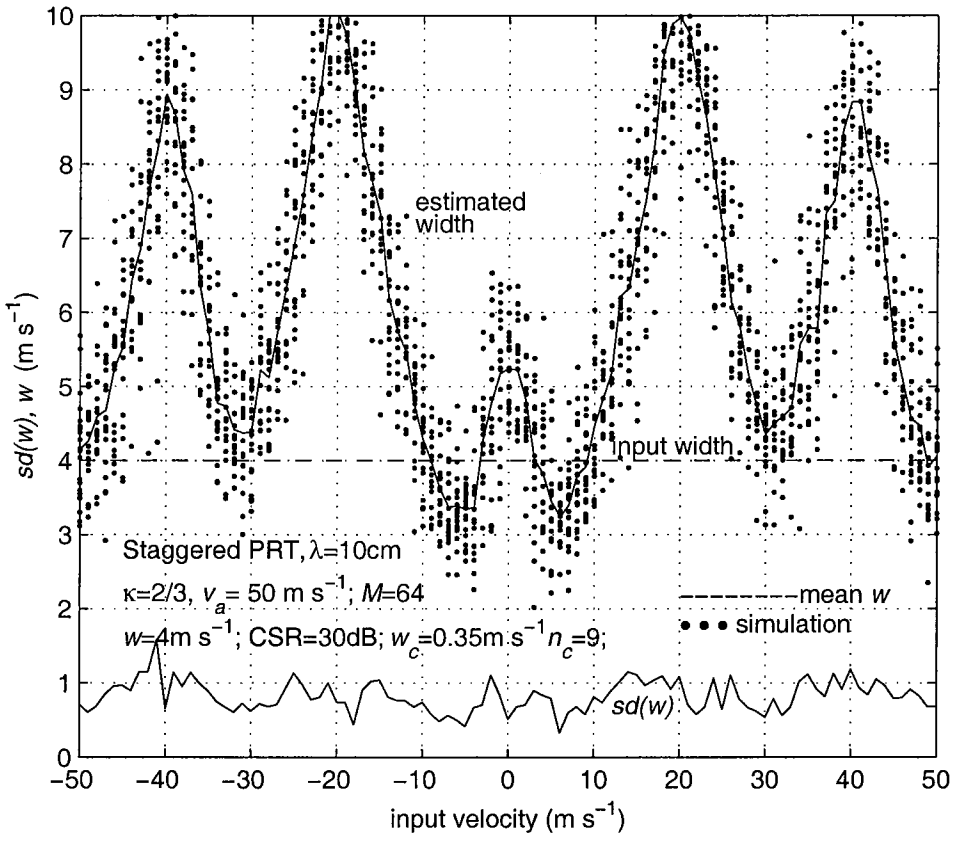

Fig. 3.13. The estimated spectrum width and the standard error in the width estimate as a function of the input velocity (input to the simulation program). Each realization is shown as a point and mean value with a continuous line.

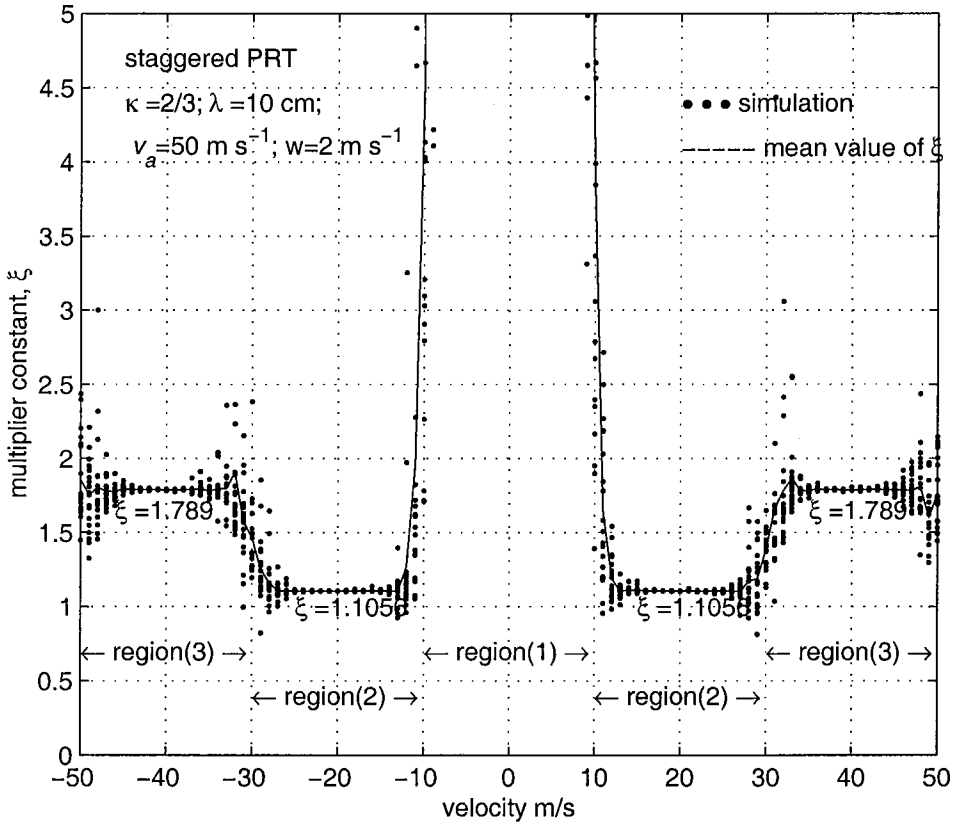

Fig. 3.14. The ratio of the actual signal amplitude to the residual amplitude after magnitude deconvolution for the spectral coefficients from which the clutter is filtered, ξ, as a function of the input velocity. Three different regions for κ=2/3 are indicated in the figure.

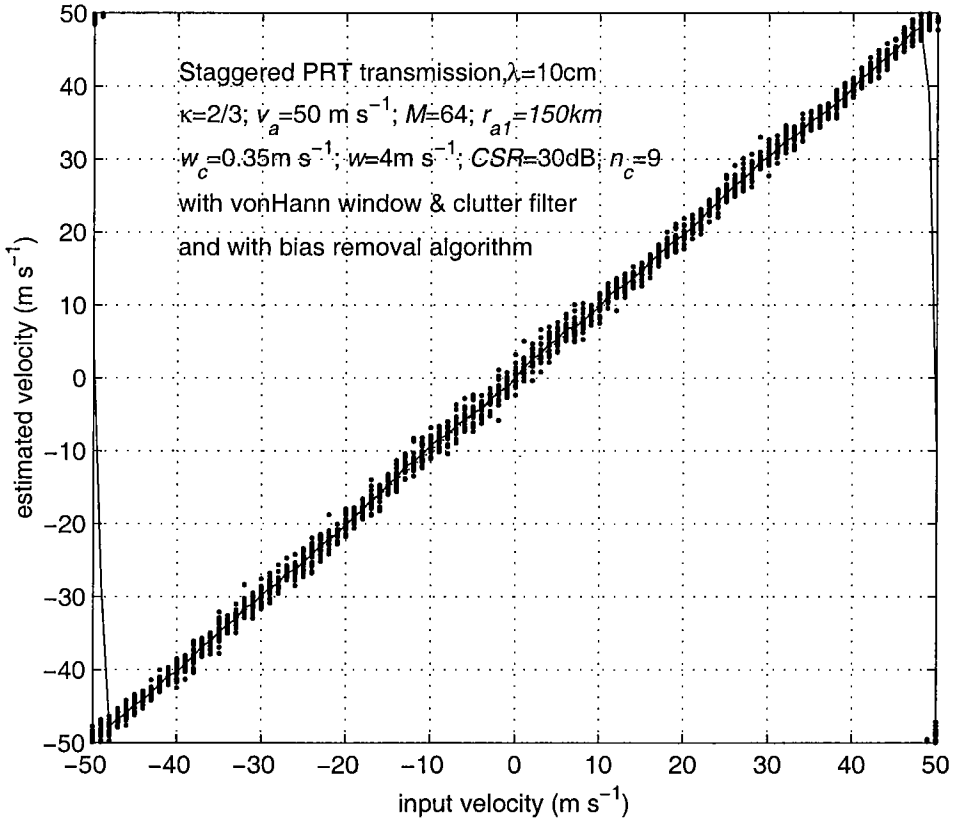

Fig. 3.15. Input velocity versus the estimated velocity using the proposed clutter filtering and bias correction algorithm. The parameters are the same as in Fig. 3.8, but with bias correction implemented in the algorithm.

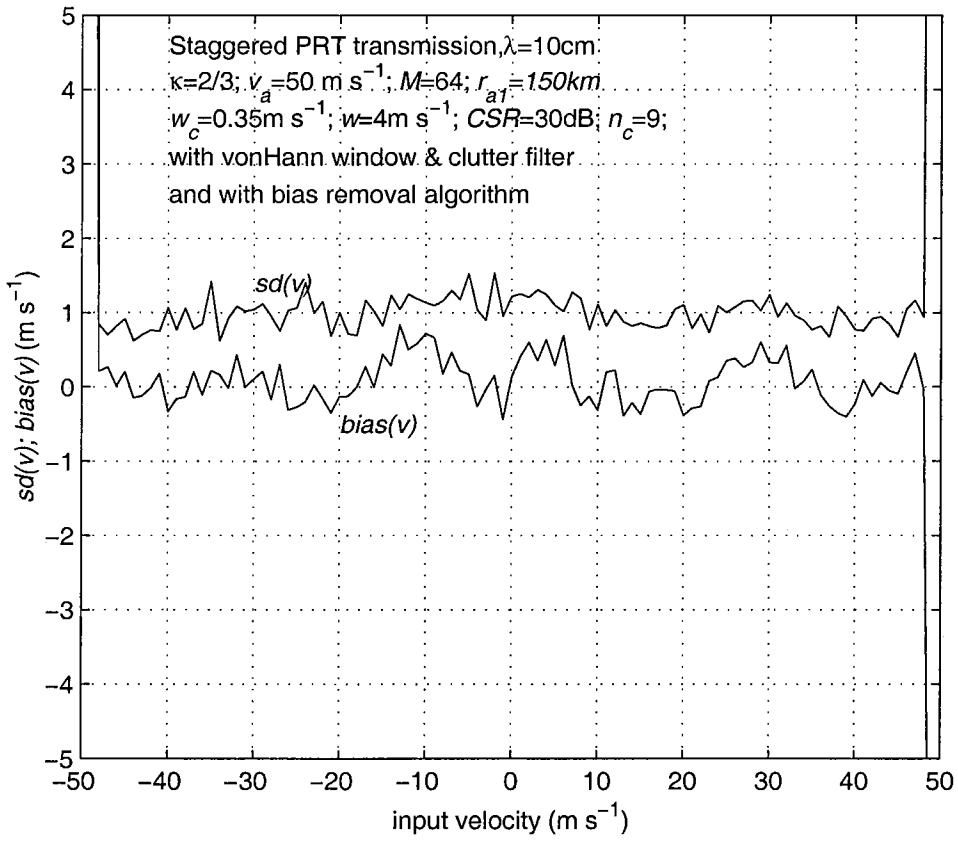

Fig. 3.16. Bias error in the velocity and the standard error in the velocity estimates using the proposed algorithm (κ=2/3) with bias correction implemented. The simulation data is the same as that in Fig. 3.15.

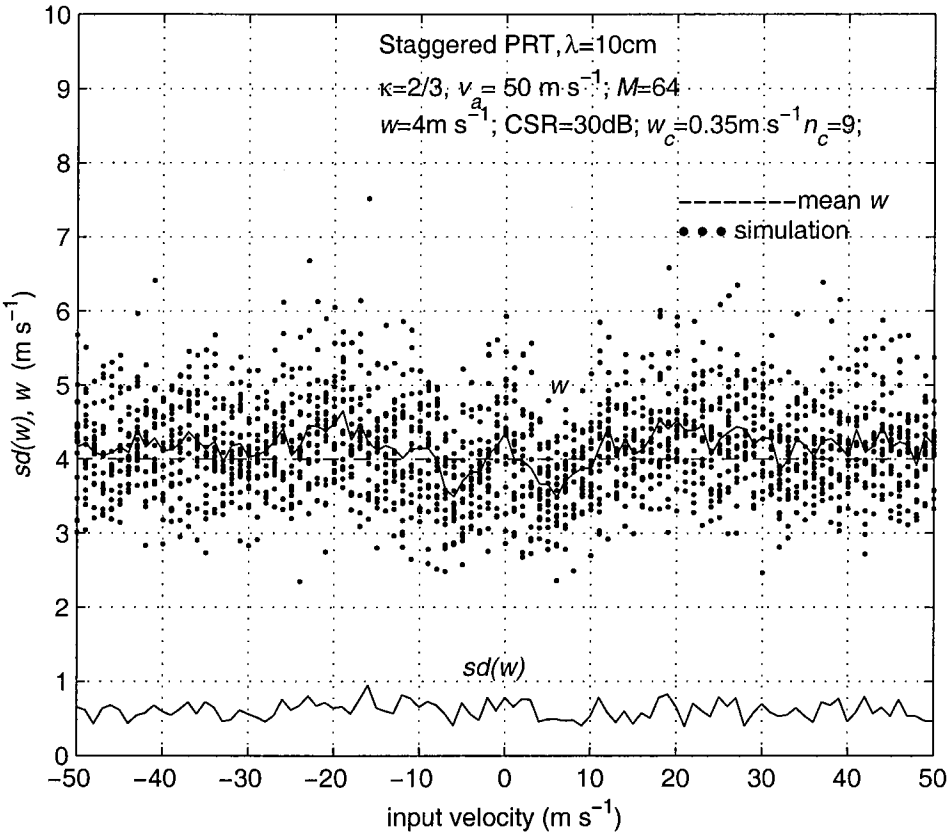

Fig. 3.17. The estimated spectrum width and the standard error in the width estimate as a function of the input velocity. This figure is similar to Fig. 3.13 with bias correction part implemented in the algorithm.

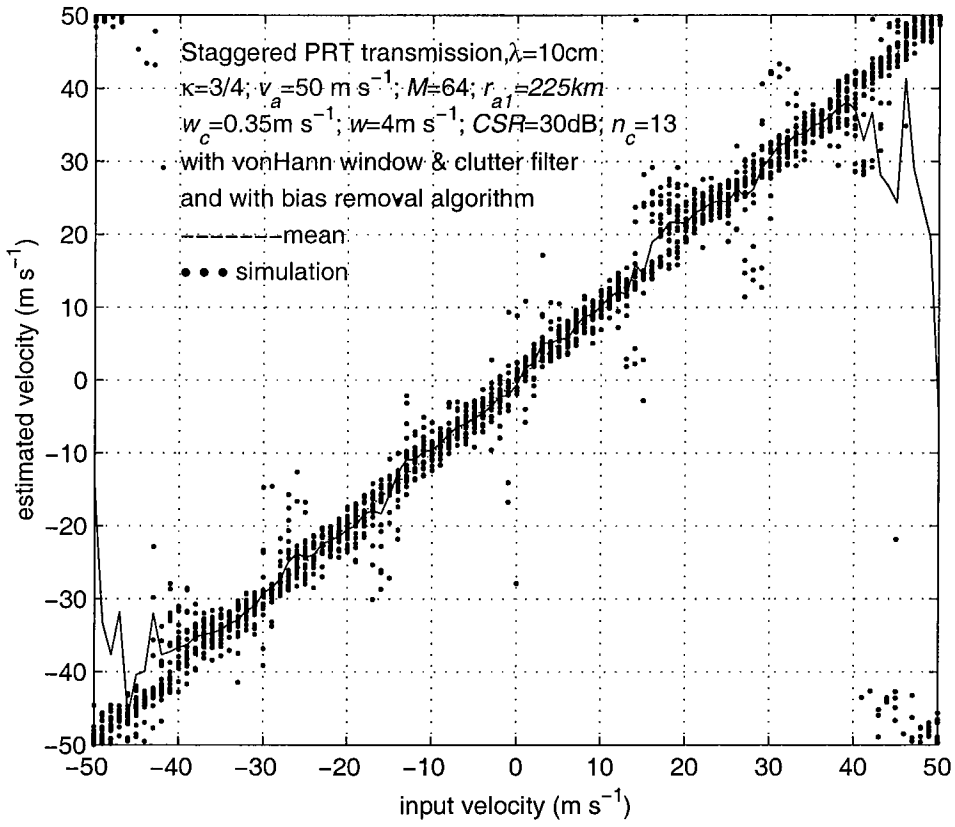

Fig. 3.18. Input velocity versus the mean of the estimated velocities using the proposed algorithm for κ=3/4. The parameters are same as that in Fig. 3.15 except for κ=3/4 and r_{a1}=225km. Both von Hann window and bias correction are included.

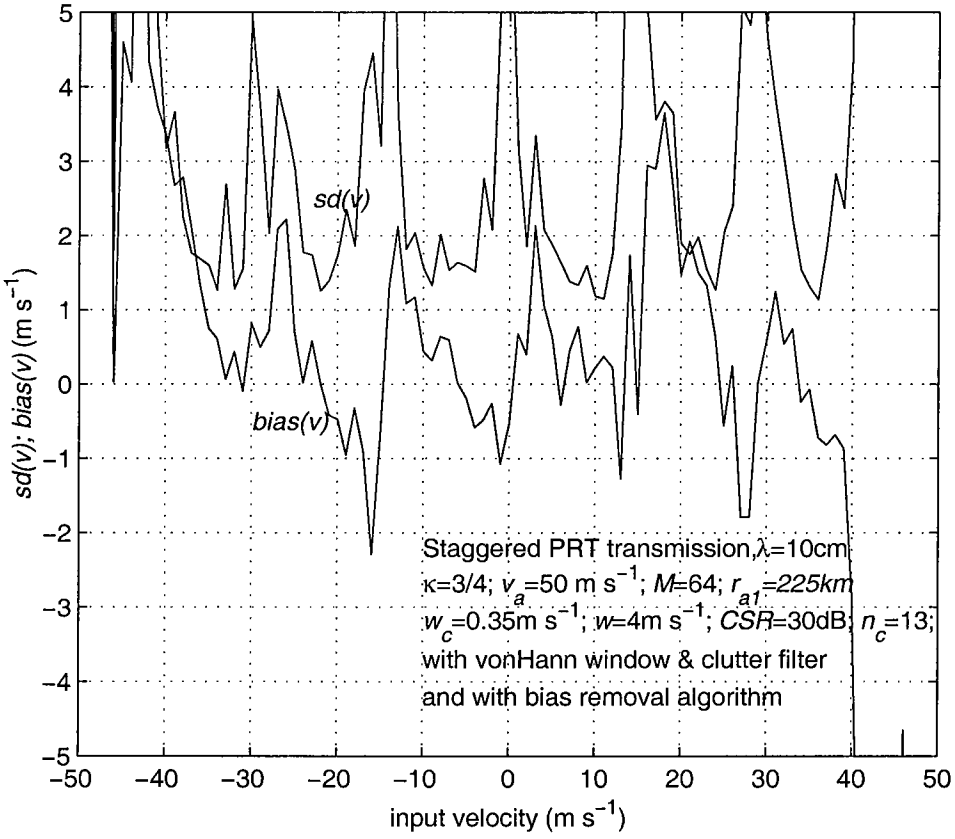

Fig. 3.19. Bias error in the velocity and the standard error in the velocity estimates using the proposed algorithm for κ=3/4 and r_{a1}=225km. The simulation data is same as that in Fig. 3.18.

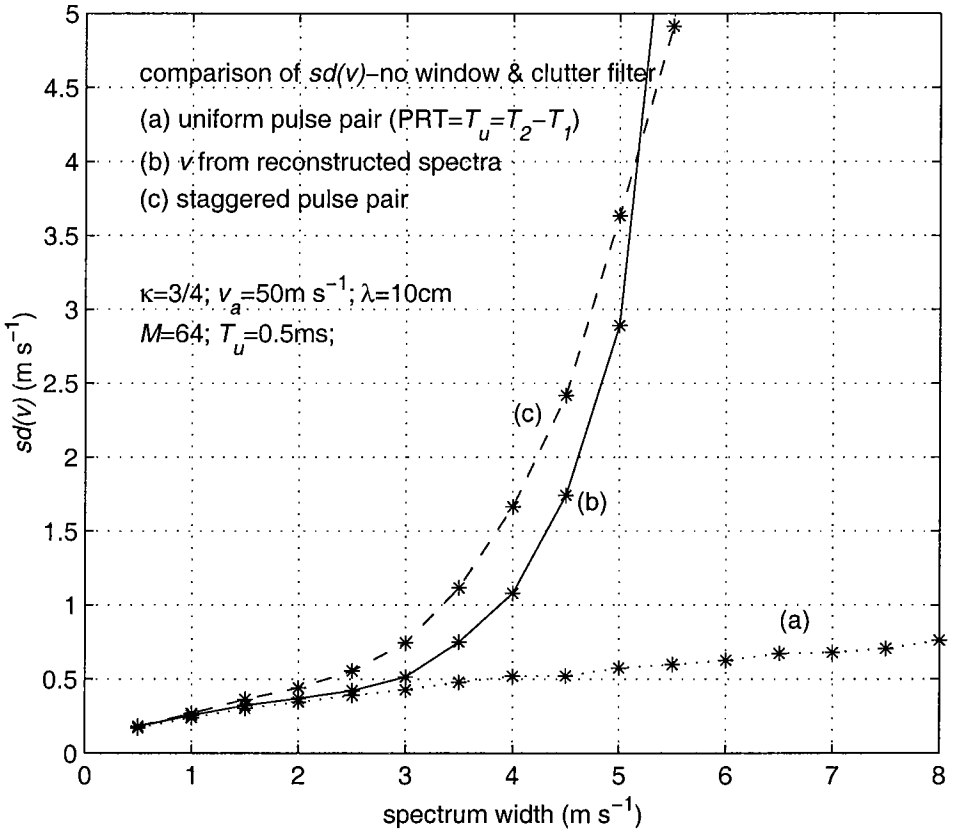

Fig. 3.20. Standard deviation of the error in the velocity estimate as a function of spectrum width of the signal for κ=3/4 (a) using complete time series samples, (b) using the reconstructed spectrum, and (c) using the ratio of $R(T_1)/R(T_2)$.

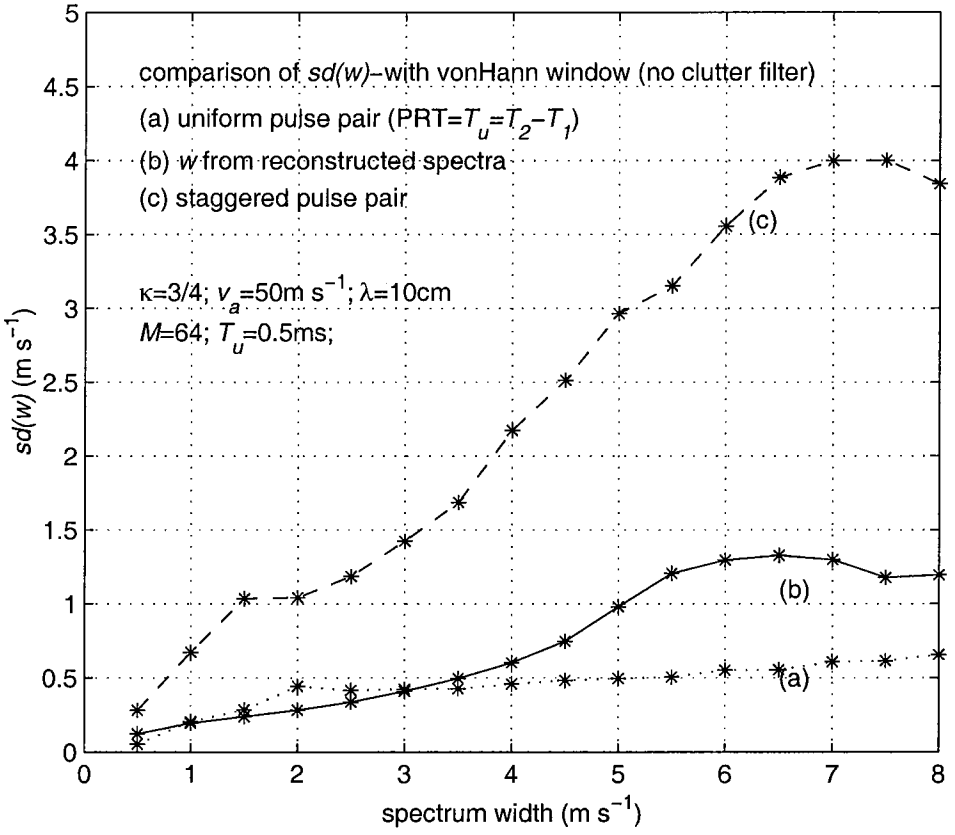

Fig. 3.21. Standard deviation of the error in the spectrum width estimate as a function of spectrum width of the signal for κ=3/4 (a) using complete time series samples, (b) using the reconstructed spectrum, and (c) using the staggered PRT samples.

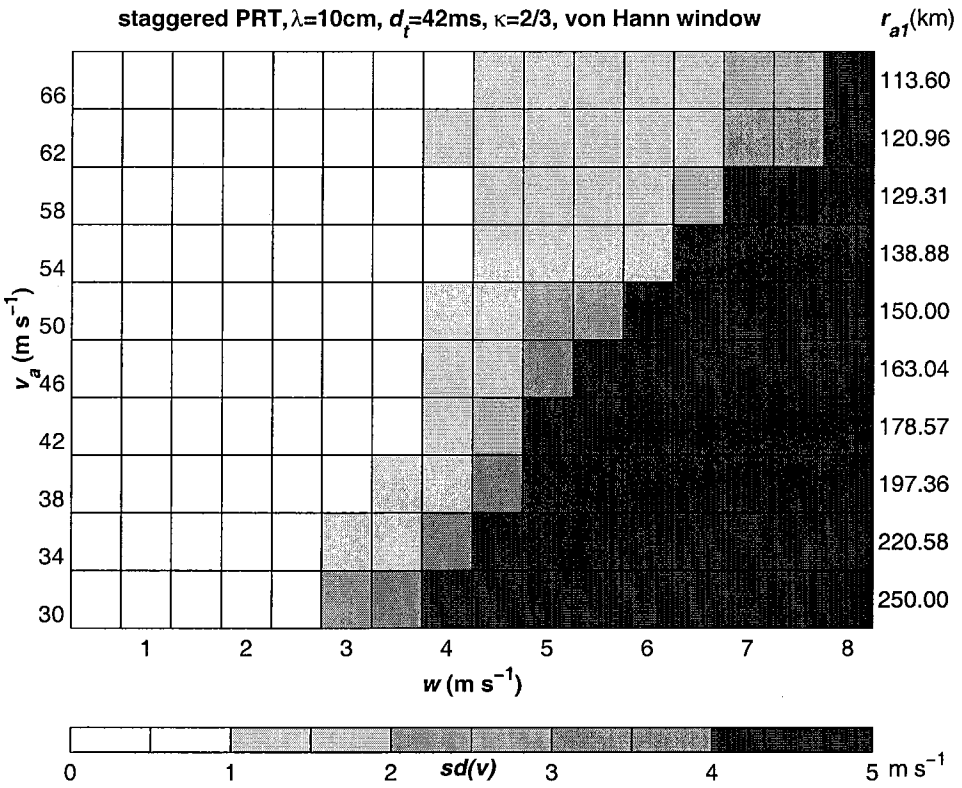

Fig. 4.1. The standard error in the velocity estimate, $sd(v)$, as a function of spectrum width of the signal, w, and the unambiguous velocity, v_a, for dwell time d_t=42ms and κ=2/3. Each value is obtained from 800 simulations (20 at each of the 40 velocity bins spread uniformly across $\pm 0.8 v_a$). $sd(v) > 5$ m/s is limited to 5m/s and quantized for plotting purposes.

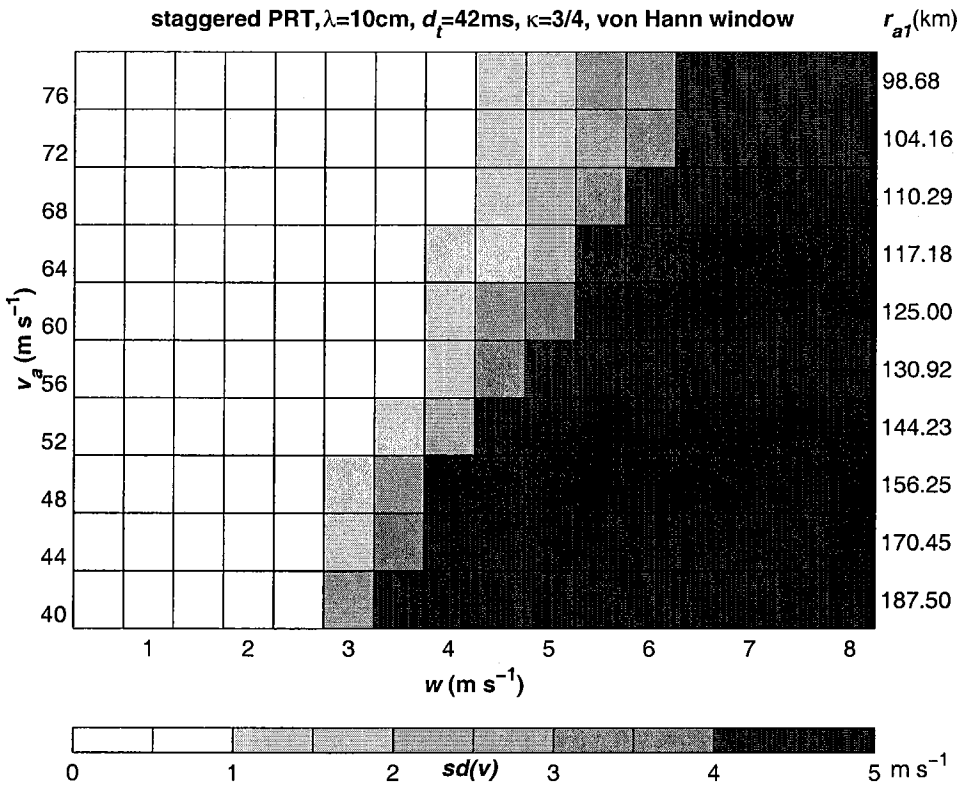

Fig. 4.2. The standard error in the velocity estimate, $sd(v)$, as a function of spectrum width of the signal, w, and the unambiguous velocity, v_a, for dwell time d_t=42ms and κ=3/4. Each value is obtained from 800 simulations (20 at each of the 40 velocity bins spread uniformly across $\pm 0.8 v_a$). $sd(v) > 5$ m/s is limited to 5m/s and quantized for plotting purposes.

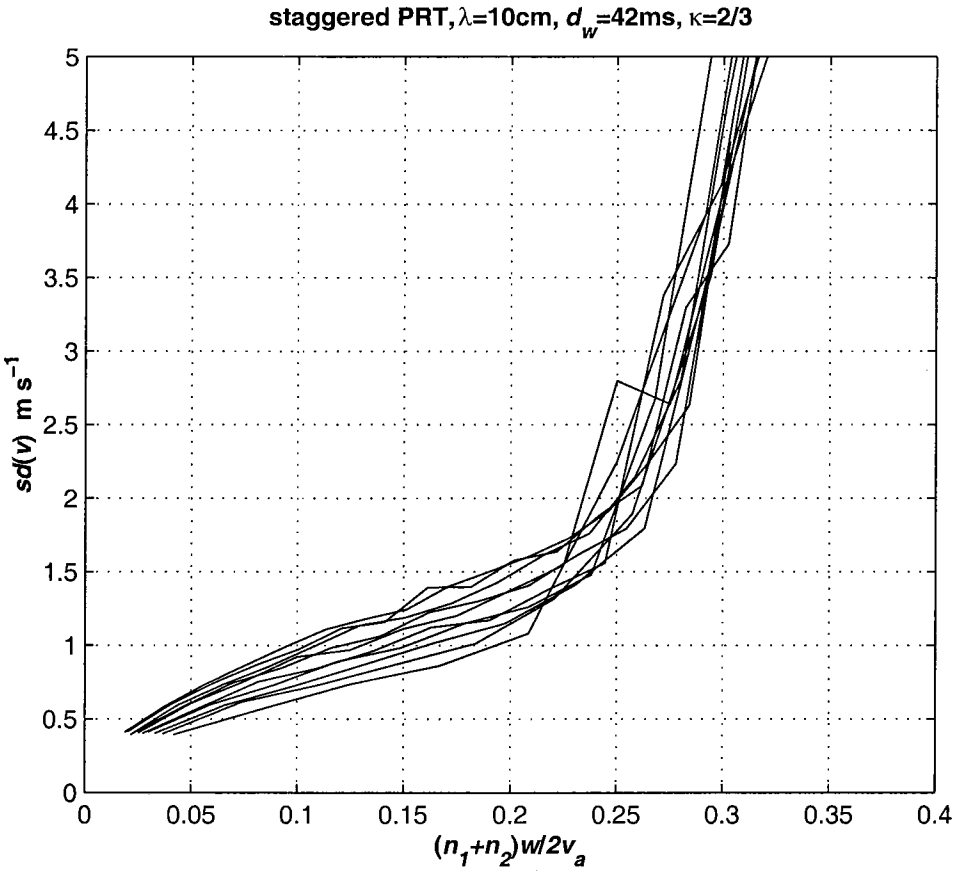

Fig. 4.3. Standard deviation of velocity estimate as a function of normalized spectrum width for the staggered PRT scheme, dwell time d_t =42 ms, and κ=2/3.

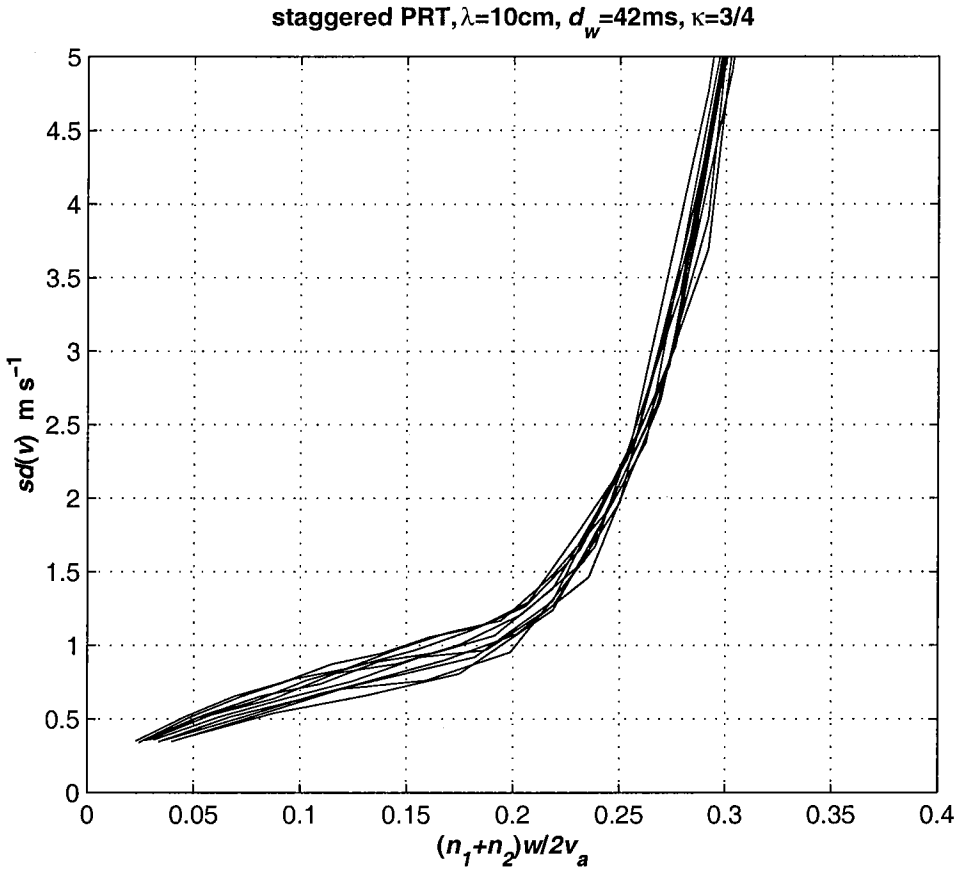

Fig. 4.4. Standard deviation of velocity estimate as a function of normalized spectrum width for the staggered PRT scheme, dwell time d_t =42 ms, and κ=3/4.

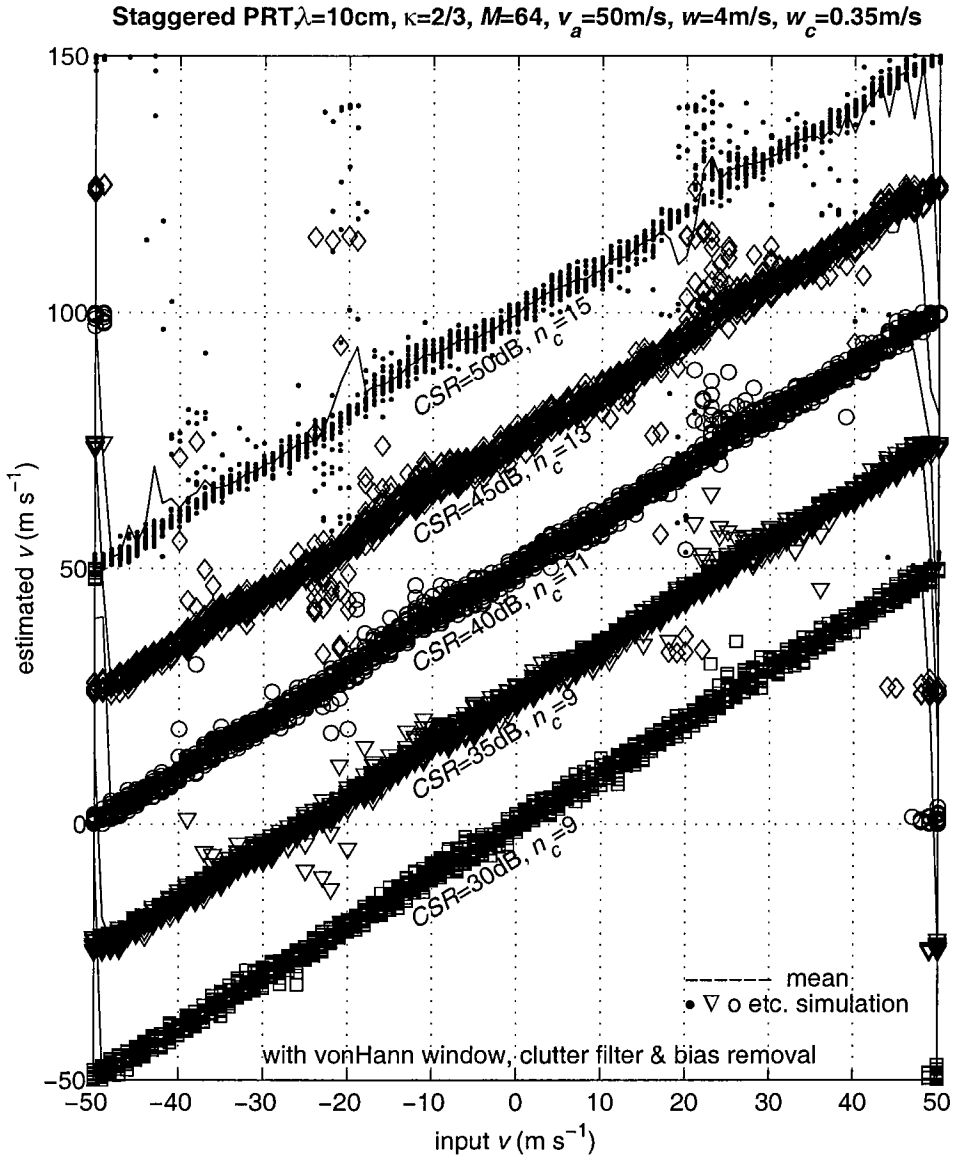

Fig. 4.5. Estimated velocity versus the input velocity with *CSR* value as a parameter for M=64 and κ=2/3. Note that the vertical scale is shifted for each CSR value by multiples of $v_a/2$, except for the lowest plot. The dots are simulation points, and the continuous curve is the mean for each input velocity.

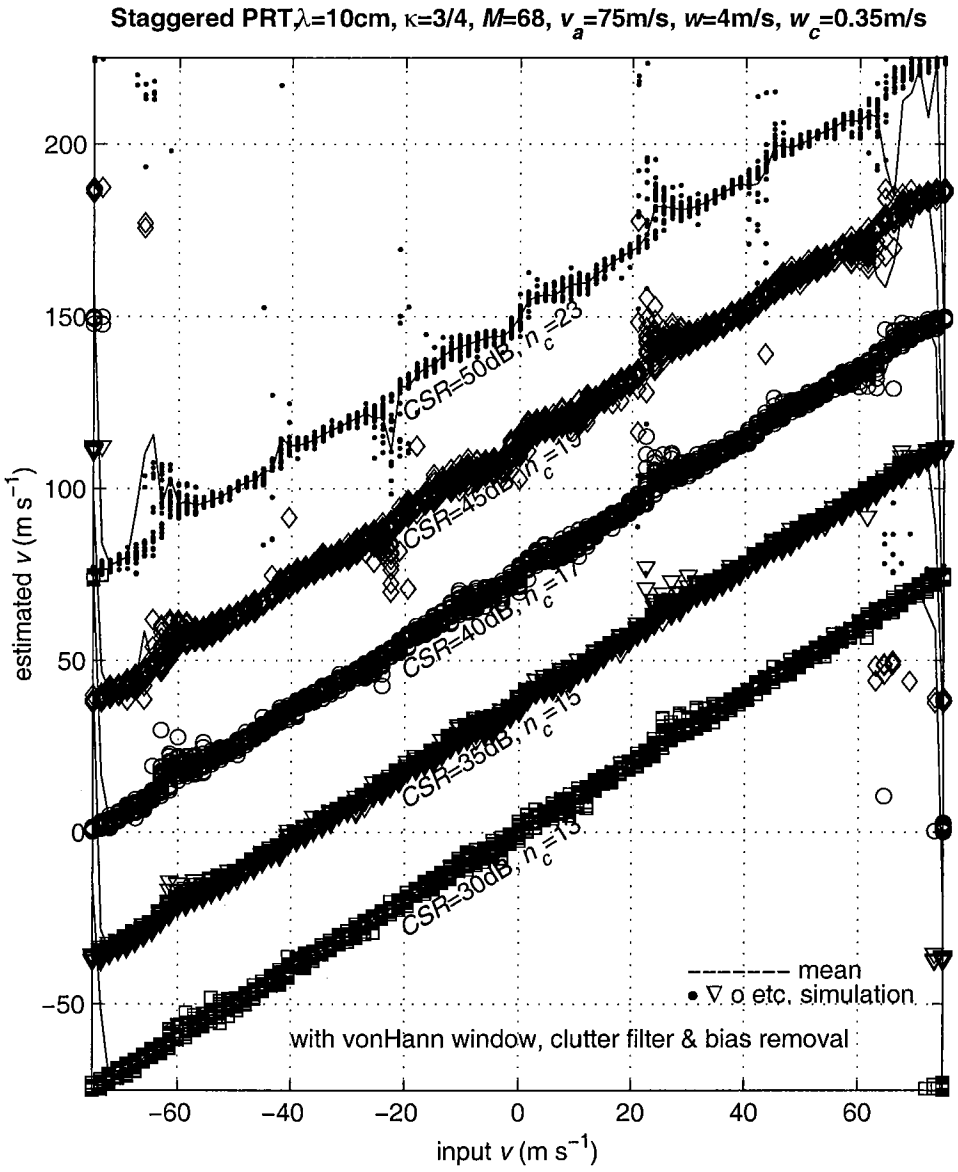

Fig. 4.6. Estimated velocity versus the input velocity with *CSR* value as a parameter for M=68 and κ=3/4. Note that the vertical scale is shifted for each CSR value by multiples of $v_a/2$, except for the lowest plot. The dots are simulation points, and the continuous curve is the mean for each input velocity.

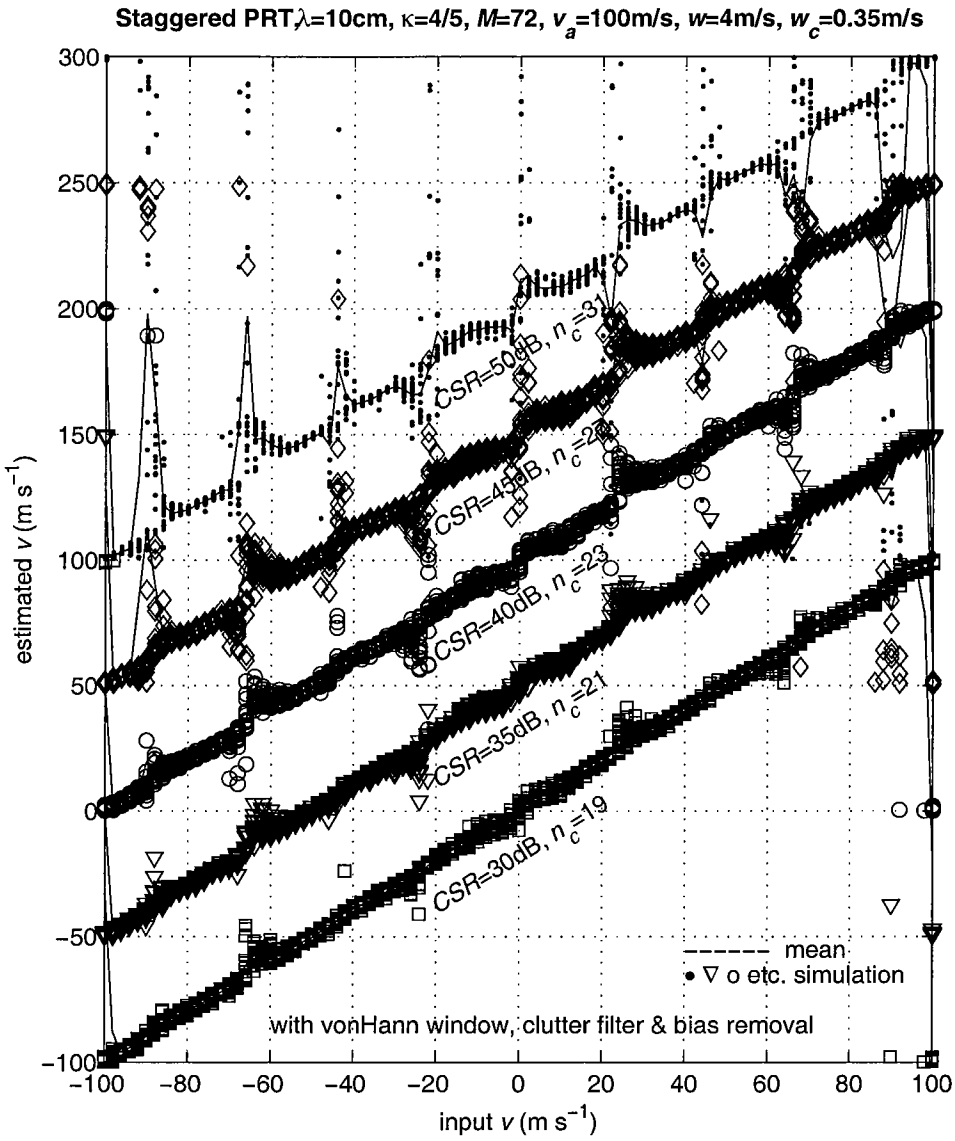

Fig. 4.7. Estimated velocity versus the input velocity with *CSR* value as a parameter for M=72 and κ=4/5. Note that the vertical scale is shifted for each CSR value by multiples of $v_a/2$, except for the lowest plot. The dots are simulation points, and the continuous curve is the mean for each input velocity.

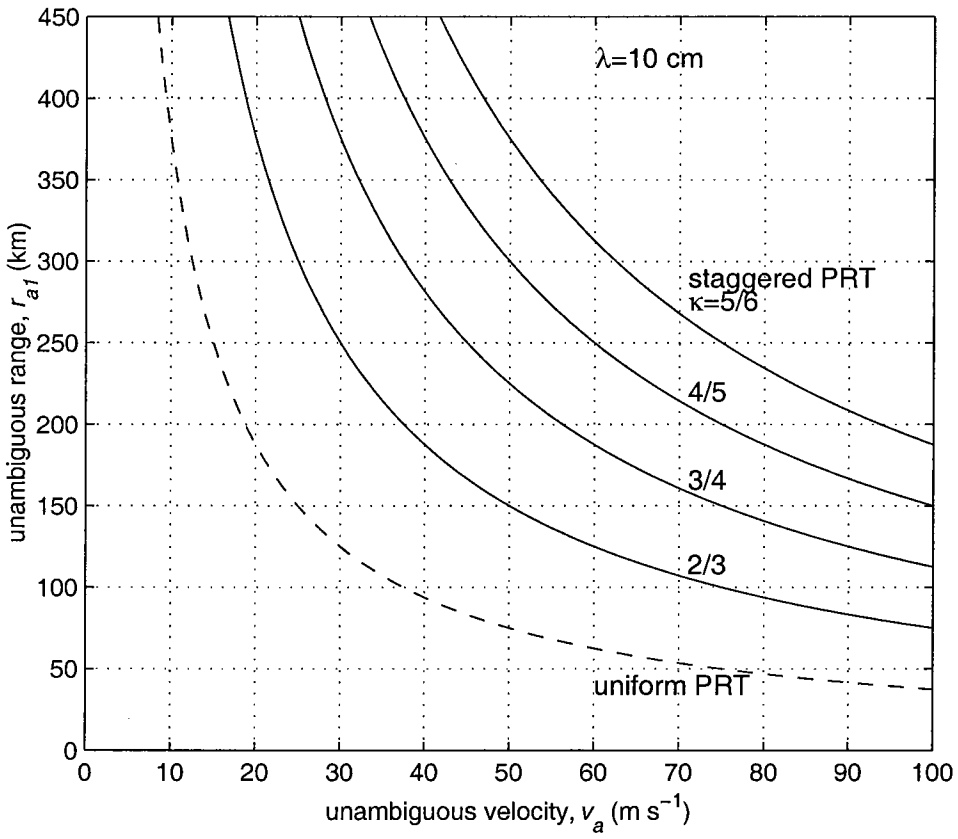

Fig. 4.8. Diagram showing the unambiguous range versus velocity for the staggered PRT scheme with the PRT ratio κ as a parameter. Curve for the uniform PRT is also shown for comparison.

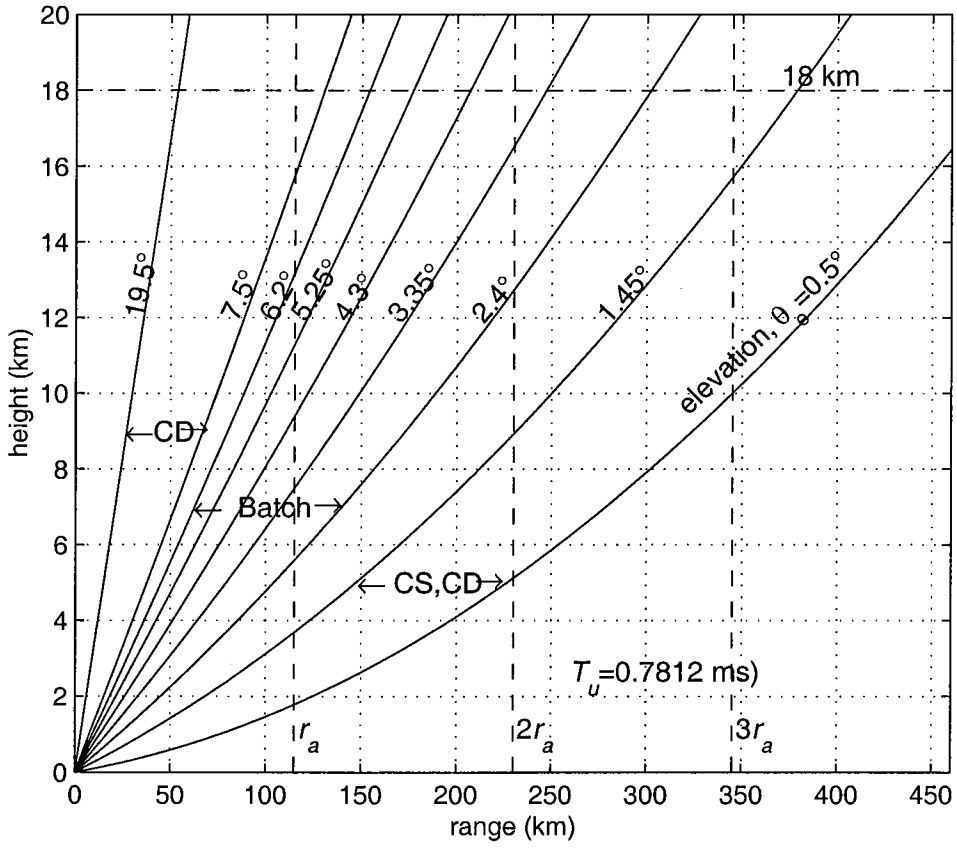

Fig. 5.1. The range-height diagram for the WSR-88D elevation scans in the VCP-11.

Table. 4.1. *sd(v)* as a function of w and v_a for d_t=42ms, κ=*2/3* staggered PRT transmission. Each value is obtained from 800 simulations (20 simulations at each of the 40 velocity bins spread uniformly across $\pm 0.8 v_a$.) Units are m s^{-1}. (Data for Fig.4.1).

$v_a \backslash w$	0.50	1.00	1.50	2.00	2.50	3.00	3.50	4.00
30	0.39	0.57	0.74	0.86	1.08	2.25	3.93	7.68
34	0.40	0.61	0.73	0.87	1.01	1.32	1.89	3.51
38	0.40	0.59	0.72	0.87	1.02	1.15	1.41	1.79
42	0.41	0.60	0.73	0.89	0.98	1.15	1.26	1.48
46	0.40	0.58	0.75	0.84	0.96	1.12	1.17	1.38
50	0.40	0.61	0.75	0.92	0.97	1.11	1.20	1.37
54	0.41	0.58	0.74	0.85	0.98	1.06	1.22	1.30
58	0.39	0.59	0.73	0.85	0.99	1.13	1.19	1.28
62	0.41	0.60	0.74	0.87	0.97	1.12	1.16	1.39

$v_a \backslash w$	4.50	5.00	5.50	6.00	6.50	7.00	7.50	8.00
30	10.23	12.76	14.14	15.33	15.88	17.11	17.44	16.95
34	6.72	10.04	12.60	15.24	17.01	18.66	19.43	19.02
38	3.72	5.92	9.82	13.03	15.42	17.42	19.19	20.31
42	2.67	5.33	6.08	9.80	13.54	15.57	18.40	19.52
46	1.56	3.38	4.13	6.45	9.37	12.33	15.43	17.61
50	1.54	2.80	2.64	4.09	5.21	9.71	12.43	15.20
54	1.40	1.61	1.79	2.23	4.22	5.40	9.02	11.38
58	1.43	1.61	1.76	2.15	2.81	4.70	6.28	6.79
62	1.40	1.58	1.64	1.89	2.09	3.29	3.73	5.72

Table. 4.2. $sd(v)$ as a function of w and v_a for d_t=42 ms, κ=3/4 staggered PRT transmission. Each value is obtained from 800 simulations (20 simulations at each of the 40 velocity bins spread uniformly across $\pm 0.8 v_a$.) Units are m s^{-1}. (Data for Fig.4.2).

$v_a \backslash w$	0.50	1.00	1.50	2.00	2.50	3.00	3.50	4.00
40	0.36	0.54	0.66	0.81	1.24	2.38	5.70	8.97
44	0.35	0.52	0.70	0.76	0.95	1.67	3.39	6.65
48	0.36	0.51	0.67	0.80	0.92	1.30	2.36	4.77
52	0.35	0.52	0.64	0.77	0.90	1.08	1.46	2.67
56	0.36	0.52	0.64	0.76	0.92	0.97	1.27	1.97
60	0.36	0.53	0.64	0.81	0.88	1.00	1.21	1.57
64	0.35	0.53	0.66	0.74	0.89	0.95	1.07	1.39
68	0.35	0.51	0.61	0.76	0.87	0.97	1.10	1.26
72	0.34	0.51	0.66	0.77	0.84	0.97	1.09	1.17

$v_a \backslash w$	4.50	5.00	5.50	6.00	6.50	7.00	7.50	8.00
40	13.25	16.62	18.75	20.49	21.53	22.42	22.69	22.37
44	10.72	13.90	17.83	20.64	21.17	22.60	24.65	24.47
48	8.25	11.95	15.03	18.92	20.33	23.33	24.82	25.51
52	4.91	8.44	11.86	16.40	20.06	22.87	25.66	26.24
56	3.76	5.78	9.62	14.40	17.06	20.67	22.85	25.90
60	2.49	3.69	7.27	10.63	15.10	18.83	21.51	25.60
64	2.07	2.90	5.16	8.34	11.31	14.82	19.49	23.19
68	1.65	2.38	3.77	5.84	8.04	13.25	16.19	20.53
72	1.48	1.89	2.63	3.91	7.14	9.80	13.93	17.36

Table. 5.1a. The WSR-88D volume coverage pattern, vcp-11.

Specification Number DV1208262D
Code Identification 56232
12 September 1994

volume coverage pattern-11 scan strategy - 1 short pulse

scan				surveillance		Doppler PRF #.				
Elevation (deg)	AZ rate (deg/sec)	Period (sec)	WF Type	PRF #	No. of pulses	4 No. of pulses	5 No. of pulses	6 No. of pulses	7 No. of pulses	8 No. of pulses
0.5	18.7	19.38	CS	1	17	-	-	-	-	-
0.5	19.2	18.83	CD	-	-	44	52	56	61	66
1.45	19.8	18.24	CS	1	16	-	-	-	-	-
1.45	19.2	18.83	CD	-	-	44	52	56	61	66
2.4	16.1	22.46	B	1	6	35	41	43	46	50
3.35	17.9	20.23	B	2	6	35	41	43	46	50
4.3	17.9	20.23	B	2	6	35	41	43	46	50
5.25	17.5	20.73	B	3	10	35	41	43	46	50
6.2	17.5	20.73	B	3	10	35	41	43	46	50
7.5	25.2	14.38	CD	-	-	34	41	43	46	50
8.7	25.4	14.25	CD	-	-	33	41	43	46	50
10.0	25.4	14.24	CD	-	-	33	41	43	46	50
12.0	25.5	14.22	CD	-	-	33	41	43	46	50
14.0	25.5	14.19	CD	-	-	33	41	43	46	50
16.7	25.6	14.14	CD	-	-	33	41	43	46	50
19.5	25.7	14.09	CD	-	-	33	41	43	46	50

Default Doppler PRF numbers are shaded.
Abbreviations: CS - contiguous surveillance.
CD - contiguous Doppler.
B - batch mode.

Table. 5.1b. The WSR-88D transmitter power and timing parameters.

Transmitter peak power	Transmitter loss	Antenna peak power
750 kW	1.6 to 2.0 dB	520 to 475 kW

PRF #	PRF (Hz)	PRT (μs.)	v_a (m s^{-1})	Duty cycle x(10^3)	
				τ = 1.57 μs.	τ = 4.5 μs.
1	321.89	3106.7	8.05	0.5	1.45
2	446.43	2240.0	11.24	0.7	2.01
3	643.78	1553.3	16.09	1.01	
4	857.14	1166.7	21.43	1.35	
5	1013.51	986.7	25.34	1.59	
6	1094.89	913.3	27.37	1.72	
7	1181.10	846.7	29.52	1.85	
8	1282.05	780.0	32.05	2.01	

Note: The WSR-88D has 5 PRF deltas. Delta C is the mid value, with A and E extremes varying by ± 1.7 %. Pulse widths are nominal with variation of about ± 4 %. Engineering parameter variation could combine to produce a variation in the above duty cycle of about ± 5 %.

Table. 5.1c. The WSR-88D volume coverage pattern, vcp-11
(Standard errors and dwell times for default PRTs.)

Specification Number DV1208262D
Code Identification 56232
12 September 1994

volume coverage pattern-11 scan strategy - 1 short pulse

scan				CS,CD scans		dwell time (ms)			[3] Standard errors		
Elev. (deg)	AZ rate (°/sec)	Period (sec)	WF Type	PRF [1] #	No. of pulses	CS scan	CD scan	v_a (m s^{-1})	[2] *sd(p)* (dB)	*sd(v)* (m s^{-1})	*sd(w)* (m s^{-1})
0.5	18.7	19.38	CS	1	17	53	-	8.05	1.12	-	-
0.5	19.2	18.83	CD	5	52	-	51.3	25.34	-	0.72	0.62
1.45	19.8	18.24	CS	1	16	50	-	8.05	1.2	-	-
1.45	19.2	18.83	CD	5	52	-	51.3	25.34	-	0.72	0.62
2.4	16.1	22.46	B	1, 5	6, 41	18.4	40.4	25.34	2.0, 1.3	0.9	0.66
3.35	17.9	20.23	B	2, 5	6, 41	13.4	40.4	25.34	2.2, 1.3	0.9	0.66
4.3	17.9	20.23	B	2 ,5	6, 41	13.4	40.4	25.34	2.2, 1.3	0.9	0.66
5.25	17.5	20.73	B	3, 5	10, 41	15.3	40.4	24.34	2.1, 1.3	0.9	0.66
6.2	17.5	20.73	B	3, 5	10, 41	15.3	40.4	25.34	2.1, 1.3	0.9	0.66
7.5	25.2	14.38	CD	6	43	-	42.4	27.37	1.2	0.87	0.64
8.7	25.4	14.25	CD	7	46	-	42	29.52	1.3	0.85	0.62
10.0	25.4	14.24	CD	7	46	-	42	29.52	1.3	0.85	0.62
12.0	25.5	14.22	CD	7	46	-	42	29.52	1.3	0.85	0.62
14.0	25.5	14.19	CD	7	46	-	42	29.52	1.3	0.85	0.62
16.7	25.6	14.14	CD	7	46	-	42	29.52	1.3	0.85	0.62
19.5	25.7	14.09	CD	7	46	-	42	29.52	1.3	0.85	0.62

Notes:
(1) The default Doppler PRF numbers are used.
(2) The *sd(p)* pair is for the long and short PRT; *sd(v)* and *sd(w)* are for the short PRT.
(3) The standard errors are computed for spectrum width, w=4m s^{-1}.
Abbreviations: CS - contiguous surveillance.
CD - contiguous Doppler.
B - batch mode.

Table.5.2. Scan parameters for staggered PRT scheme(κ=2/3).

elv (deg)	dwell (ms)	AZ rate (°/sec)	range (km)[1]	T_1 (ms)	T_u (ms)	M	v_a (m s^{-1})	$2v_a/5$ (m s^{-1})	w(max) (m s^{-1})[2]
0.50	104.3	9.42	460	3.07	1.53	34	16.30	6.52	1.86
1.45	101.3	9.71	379	2.52	1.26	32	19.79	7.91	2.26
2.40	59.0	16.03	303	2.02	1.01	24	24.75	9.90	2.83
3.35	53.8	17.80	247	1.64	0.82	26	30.36	12.14	3.47
4.30	53.8	17.80	207	1.38	0.69	32	36.23	14.49	4.14
5.25	55.9	17.37	177	1.18	0.59	38	42.37	16.94	4.84
6.20	55.9	17.37	154	1.02	0.51	44	48.70	19.48	5.56
7.50	42.4	25.03	131	0.86	0.43	38	57.25	22.90	6.54
8.70	42.0	25.26	115	0.76	0.38	44	65.21	26.09	7.45
10.00	42.0	25.28	100	0.66	0.33	50	75.00	30.00	8.57
12.00	42.0	25.32	85	0.56	0.28	60	88.23	35.29	10.08
14.00	42.0	25.37	73	0.48	0.24	68	102.74	41.09	11.74
16.7	42.0	25.46	62	0.40	0.20	80	120.97	48.39	13.82
19.5	42.0	22.37	54	0.36	0.18	92	138.89	55.55	15.87

Note:
(1) The maximum range is calculated based on a maximum height of 18km for all elevations except 0.5°, for which it is 16km.
(2) The values of w(max) are calculated for M=64.

Table. 5.3. A proposed volume coverage pattern for the WSR-88D.

Proposed alternative to volume coverage pattern-11

Elev. (deg)	AZ rate (°/sec)	Period (sec)	WF Type	M	T_u [2] (ms)	v_a (m/s)	r_a (km)	standard errors[1]		
								sd(p) (dB)	*sd(v)* (m s^{-1})	*sd(w)* (m s^{-1})
0.5	18.7	19.38	CS, 1	17	3.11	-	466	1.2	-	-
0.5	19.2	18.83	SZ(8/64)	52	0.78	32.05	234	1.53, 1.87	1.02, 1.29	0.68, 1.37
1.45	19.8	18.24	CS, 1	16	3.11	-	466	1.2	-	-
1.45	19.2	18.83	SZ (8/64)	52	0.78	32.05	234	1.53, 1.87	1.02, 1.29	0.68, 1.37
2.4	16.1	22.46	SZ (8/64)	52	0.78	32.05	234	1.53, 1.87	1.02, 1.29	0.68, 1.37
3.35	17.9	20.23	SZ(8/64)	72	0.75	33.33	225	1.31, 1.88	0.85, 1.27	0.66, 1.18
4.3	17.9	20.23	SZ(8/64)	84	0.62	40.32	186	1.32, 1.52	0.9, 1.15	0.59, 1.41
5.25	17.5	20.73	ST(2/3)	38	0.59	42.37	177	1.25	0.95	0.58
6.2	17.5	20.73	ST(2/3)	44	0.51	49.02	153	1.32	0.90	0.54
7.5	25.2	14.38	ST(2/3)	38	0.44	56.82	132	1.46	1.02	0.63
8.7	25.4	14.25	ST(2/3)	44	0.38	65.79	114	1.57	0.99	0.60
10.0	25.4	14.24	ST(2/3)	52	0.33	75.76	99	1.41	1.01	0.57
12.0	25.5	14.22	ST(2/3)	60	0.28	89.29	84	1.53	1.02	0.61
14.0	25.5	14.19	ST(2/3)	60	0.28	89.29	84	1.53	1.02	0.61
6.7	25.6	14.14	ST(2/3)	60	0.28	89.29	84	1.53	1.02	0.61
19.5	25.7	14.09	ST(2/3)	60	0.28	89.29	84	1.53	1.02	0.61

Notes:

(1) For the SZ(8/64) scheme, the standard errors are computed for w_1=4 m s^{-1} and w_2=4 m s^{-1}. The standard errors pairs are for the stronger and the weaker signals; p_1/p_2=20dB. For the ST(2/3) scheme, w=4 m s^{-1} is used. The sample overlap scheme (see Rep.-2) is used to increase M by 30% in computing standard errors in both schemes.

(2) The short PRT for the ST(2/3) mode is $2T_u$. The Klystron duty cycle may limit the shortest PRT that can be used at higher elevation scans.

Abbreviations: CS - contiguous surveillance (same as the original WSR-88D scheme).
SZ(n/M) - SZ phase coded contiguous Doppler.
ST(κ) - Staggered PRT.

References.

1. Banjanin, Z.B. and D.S. Zrnic, **1991:** Clutter rejection for Doppler weather radars which use staggered pulses. *IEEE Trans. On Geoscience and Remote Sensing,* **29**, 610-620.

2. Chornoboy, E.S., **1993:** Clutter filter design for multiple PRT signals. *26th Conference on Radar Meteorology., AMS*, 235-237.

3. Chornoboy, E.S and M.E. Weber, **1994:** Variable PRI processing for meteorological Doppler radars. *Proc. of the IEEE National Radar Conference, New York, NY*, 85-90.

4. Doviak, R.J. and D. Sirmans, **1973**: Doppler radar with polarization diversity., *J. Atmos. Sci.,* **30**, 737-738.

5. Doviak, R.J. and D.S. Zrnic, **1993**: *Doppler Radar and Weather Observations.*, Academic Press, New York, 562pp.

6. Laird, B.G., **1981**: On ambiguity resolution by random phase processing., *20th Conference on Radar Meteorology., AMS*, 327-331.

7. Pirttila, J., A. Huuskonen, and M. Lehtinen, **1999:** Solving the range-Doppler dilemma with ambiguity-free measurements developed for Incoherent Scatter radars. *Cost 75, Advanced weather radar systems-International seminar*, 557-568.

8. Sachidananda, M., D.S. Zrnic, and R.J. Doviak, **1997**: Signal design and processing techniques for WSR-88D ambiguity resolution, Part-1. *National Severe Storms Laboratory*, July 1997, 100 pp.

9. Sachidananda, M., D.S. Zrnic, and R.J. Doviak, **1998**: Signal design and processing techniques for WSR-88D ambiguity resolution, Part-2. *National Severe Storms Laboratory*, June 1998, 105 pp.

10. Sebastian Torres, **1998:** Ground clutter canceling with a regression filter. *National Severe Storms Laboratory*, June 1998, 33pp.

11. Siggia, A., **1983**: Processing phase coded radar signals with adaptive digital filters., *21st Conference on Radar Meteorology., AMS*, 167-172.

12. Sirmans, D., D.S. Zrnic and W. Bumgarner, **1976:** Estimation of maximum unambiguous Doppler velocity by use of two sampling rates. *18th Conference on Radar Meteorology., AMS, Boston, MA,* 23-28.

13. Weber, M.E. and E.S.Chornoboy, **1993:** Coherent processing across multi-PRI waveforms. *26th Conference on Radar Meteorology., AMS*, 232-234.

14. Zrnic, D.S., **1979**: Random phase radar., *NSSL memorandum,* April 1979.

15. Zrnic, D.S., and P.R. Mahapatra, **1985**: Two methods of ambiguity resolution in pulsed Doppler weather radars. *IEEE Trans. on Aerospace and Electronic Systems.*, vol. **AES-21,** 470-483.

LIST OF NSSL REPORTS FOCUSED ON
POSSIBLE UPGRADES TO THE WSR-88D RADARS.

Doviak, R.J. and D.S. Zrnic, **1998:** NOAA/NSSL's WSR-88D Radar for Research and Enhancement of Operations: Polarimetric Upgrades to Improve Rainfall Measurements, 110 pp.

Sachidananda, M., **1998:** Signal Design and Processing Techniques for WSR-88D Ambiguity Resolution, Part II, 105 pp.

Sachidananda, M., **1997:** Signal Design and Processing Techniques for WSR-88D Ambiguity Resolution, Part I, 100 pp.

Sirmans, D., D.S. Zrnic, and M. Sachidananda, **1986:** Doppler radar dual polarization considerations for NEXRAD, Part I, 109 pp.

Sirmans, D., D.S. Zrnic, and N. Balakrishnan, **1986:** Doppler radar dual polarization considerations for NEXRAD, Part II, 70 pp.